Physics – Uspekhi **40** (4) 337 – 358 (1997)

REVIEWS OF TOPICAL PROBLEMS PACS numbers: 63.20.Kr, **71.10.+x**, 71.20.Cf, **71.38.+i**

The electron – phonon interaction and the physical properties of metals

E G Maksimov, D Yu Savrasov, S Yu Savrasov

Contents

1. **Introduction** 337
2. **The many-body theory of electron-phonon interaction** 338
3. **Application of the Landau Fermi-liquid theory to the electron – phonon interaction** 341
4. **The density functional method and electron – phonon interaction** 343
5. **The linear response theory and calculations of electron – phonon interactions for particular metals** 345
6. **Conclusions** 356

References 357

Abstract. Theoretical work dealing with the electron – phonon interaction (EPI) and its effects on the physical properties of metals is reviewed. The many-body approach and that using Landau's Fermi-liquid theory are briefly described and their adequacy is demonstrated for low values of the adiabaticity parameter $(\omega_D/\varepsilon_F)^{1/2}$, where ω_D is the characteristic phonon frequency, and ε_F the Fermi energy. Density functional theory as applied to EPI calculations are outlined, and for a number of simple and transition metals, the results of calculating the EPI spectral densities and EPI-dependent physical properties are presented. The potentialities and the range of validity for EPI applications of the density functional method are discussed.

1. Introduction

Electron – phonon interaction (EPI) in metals is a subject of intensive theoretical and experimental investigation. Interest in this problem is associated with the role of electron – phonon interaction in the description of such fundamental physical phenomena as superconductivity and transfer processes in metals. A consistent many-body EPI theory has been developed to describe both normal and superconducting states of metals (see Refs [1 – 4]). Within this approach all the phenomena caused by EPI are expressed in terms of the so-called EPI spectral densities. One of them, namely the Eliashberg function describing the changes in one-particle properties of electrons in the normal state and the phonon contribution to superconductivity can be determined experimentally. It can be regenerated from the dependence of the tunnelling current flowing between a normal metal and a superconductor on the voltage applied [5]. The Eliashberg function is correctly determined only for superconducting metals and is difficult to evaluate for anisotropic superconductors and superconductors with short coherence length.

It would be desirable to calculate the EPI spectral densities by a consistent microscopic approach. Such efforts were made earlier (see Ref. [2]), but they were inconsistent in many respects. As will be evident from the subsequent discussion, in order to calculate the EPI spectral densities, one should know the electron and phonon excitation spectra and the EPI matrix element. In many earlier attempts at EPI microscopic calculations the phonon spectra of metals were not calculated *ab initio*. Instead, they were determined by various phenomenological models such as the Born – Karman model of force constants. The EPI matrix elements were also obtained with the help of various simplified approaches such as the model of the rigid muffin-tin potential [6]. But perhaps, the most essential problem, however, omitted in earlier discussions, was concerned with the choice of an electron spectrum to be used in these calculations.

In most papers on EPI calculation a spectrum found by the density functional theory (DFT) was used as an electron spectrum [7, 8]. It is well known [9] that the conventional DFT is intended to describe the properties of the ground state of interacting systems. In this regard, the suitability of the DFT for calculation of phonon spectra is beyond question. The point is that in order to calculate the phonon spectrum within the adiabatic approximation, one should find the ground state energy of the electron subsystem as a function of ion coordinates. For this purpose the DFT has rather powerful and effective tools based on the static linear response theory. These methods have enabled the phonon calculations for a wealth of metals, the results being in agreement with the experimental data [10].

The situation with microscopic calculations of electron – phonon interaction and related effects such as electrical resistivity and thermal conductivity is quite different. These effects are not conditioned by the ground state. There are two ways for the microscopic calculation of these phenomena. On the one hand, one can use a recent method of a time-

E G Maksimov, D Yu Savrasov P N Lebedev Physical Institute, Russian Academy of Sciences, Leninskiĭ prosp. 53, 117924 Moscow, Russia
Tel. (7-095) 135 75 11
Fax (7-095) 135 85 33
E-mail: maksimov@lpi.ac.ru, savrasov@lpi.ac.ru
S Yu Savrasov Max-Planck Institut, 70569 Stuttgart, Germany

Received 18 December 1996
Uspekhi Fizicheskikh Nauk **167** (4) 353 – 376 (1997)
Translated by G N Chuev; edited by A Radzig

dependent density functional (see Ref. [11]). Formally, a set of equations describing a system of interacting electrons and phonons in an external field has rather a simple form. But actually, neither exact nor even approximate expressions have been obtained as yet for the dependences of the exchange-correlation energy on the ion density. However it is this dependence that determines the electron – phonon interaction and its influence on the properties of the electron system. The other way implies the description of the effects of electron – phonon interaction by the so-called Fermi-liquid approach. In this paper we will deal with this particular approach. The paper is arranged as follows. First, we present the results of a many-body treatment of the EPI effects within the framework of the Fröhlich Hamiltonian. We describe the ways of deriving this Hamiltonian by the Landau Fermi-liquid theory and discuss the possible evaluation of the Hamiltonian parameters by the functional density method. Then we present the EPI spectral densities and the physical properties calculated for a number of metals. In conclusion we discuss the possibilities of further development of methods for EPI calculation.

2. The many-body theory of electron – phonon interaction

The many-body EPI theory is presented in numerous books and reviews and we will not dwell upon it at length. We will only recall here the main facts of the theory and some formulas, which will be used in the subsequent discussion. To start with, notice that in the many-body theory the electron – phonon interaction is usually described by the so-called Fröhlich Hamiltonian

$$H = H_{\mathrm{e}} + H_{\mathrm{ph}} + H_{\mathrm{e-ph}} \,. \tag{1}$$

Here H_{e} presents quasi-stationary electron states in a rigid lattice:

$$H_{\mathrm{e}} = \sum_{\mathbf{k}} \varepsilon_{\mathbf{k}} c_{\mathbf{k}}^{+} c_{\mathbf{k}} \,, \tag{2}$$

where $\varepsilon_{\mathbf{k}}$ is the energy of electron quasi-particles, $c_{\mathbf{k}}^{+}$ and $c_{\mathbf{k}}$ are the operators of creation and annihilation of the quasi-particles; H_{ph} is the Hamiltonian of noninteracting phonons

$$H_{\mathrm{ph}} = \sum_{\mathbf{q},\,\nu} \omega_{\mathbf{q}\nu} \left(b_{\mathbf{q}\nu}^{+} b_{\mathbf{q}\nu} + \frac{1}{2} \right) , \tag{3}$$

where $\omega_{\mathbf{q}\nu}$ is the energy of a phonon with the polarization ν, $b_{\mathbf{q}\nu}^{+}$ and $b_{\mathbf{q},\nu}$ are the corresponding phonon operators; $H_{\mathrm{e-ph}}$ is the Hamiltonian of electron – phonon interaction

$$H_{\mathrm{e-ph}} = \sum_{\mathbf{k},\,\mathbf{q},\,\nu} g_{\mathbf{k}+\mathbf{q},\,\mathbf{k}}^{\mathbf{q}\nu} c_{\mathbf{k}+\mathbf{q}}^{+} c_{\mathbf{k}} (b_{-\mathbf{q}\nu}^{+} + b_{\mathbf{q}\nu}) \,, \tag{4}$$

where $g_{\mathbf{k}+\mathbf{q},\,\mathbf{k}}^{\mathbf{q}\nu}$ is the EPI matrix element. Later on we will discuss in greater detail the use of the Fröhlich Hamiltonian in describing EPI and calculating the functions involved, such as the electron and phonon energies and the EPI matrix element.

Now let us consider the EPI computations with the use of the Fröhlich Hamiltonian. The many-body electron – phonon interactions are usually calculated by Green's function method. Treatment of this method is outside the scope of this paper: for details the reader is referred to [1, 12], where the method is thoroughly analyzed. The EPI were first calculated with the help of Green's functions by Migdal [13] for the normal metal state and by Eliashberg [14] for the superconducting state. We will start our consideration with temperature $T = 0$, since in this case all the relevant formulas have rather a simple form and enable the easy introduction of appropriate EPI spectral functions. The electron Green's function $G(\mathbf{k}, \omega)$ and the phonon Green's function $D(\mathbf{q}, \nu, \omega)$ can be written in terms of electron $\Sigma(\mathbf{k}, \omega)$ and phonon $\Pi(\mathbf{q}, \nu, \omega)$ self-energy parts as

$$G^{-1}(\mathbf{k}, \omega) = G_0^{-1}(\mathbf{k}, \omega) - \Sigma(\mathbf{k}, \omega) \,, \tag{5}$$

$$D^{-1}(\mathbf{q}, \nu, \omega) = D_0^{-1}(\mathbf{q}, \nu, \omega) - \Pi(\mathbf{q}, \nu, \omega) \,. \tag{6}$$

Here $G_0(\mathbf{k}, \omega)$ is the Green's function of noninteracting electrons, given by the Hamiltonian H_{e}:

$$G_0(\mathbf{k}, \omega) = \frac{1}{\omega - \varepsilon_{\mathbf{k}} + \mathrm{i}\delta} \,. \tag{7}$$

Function $D_0(\mathbf{q}, \nu, \omega)$ is determined by the Hamiltonian H_{ph} and has the form

$$D_0(\mathbf{q}, \nu, \omega) = \frac{2\omega_{\mathbf{q}\nu}}{\omega^2 - \omega_{\mathbf{q}\nu}^2 + \mathrm{i}\delta} \,. \tag{8}$$

To anticipate, in the general case the self-consistent calculation of electron and phonon Green's functions with the Fröhlich Hamiltonian cannot be rigorously justified. The exact $D(\mathbf{q}, \nu, \omega)$ function must be calculated using the total electron-ion Hamiltonian. However, in a number of problems one can employ the Fröhlich Hamiltonian for self-consistent calculation of both Green's functions as well, having specified bare phonons in the function $D_0(\mathbf{q}, \nu, \omega)$. In any case, the phonon damping defined by the imaginary part of the phonon self-energy $\Pi(\mathbf{q}, \nu, \omega)$ is determined properly by this Hamiltonian (see Ref. [15]). In what follows we will not concentrate on calculations of the phonon Green's function, assuming it to be exact in all the formulas concerned with electron properties resulted in turn from electron – phonon interactions. A detailed procedure for microscopic calculations of exact phonon spectra in metals was given in Ref. [10].

One of the main results of Migdal's paper is that the electron self-energy can be calculated with regard to the simplest first-order EPI contributions neglecting the higher-order terms as being small relative to $\omega_{\mathrm{D}}/\varepsilon_{\mathrm{F}}$. Here ω_{D} is a characteristic phonon frequency and ε_{F} is the Fermi energy. The analytical expression for $\Sigma(\mathbf{k}, \omega)$ can be given as

$$\Sigma(\mathbf{k}, \omega) = \mathrm{i} \sum_{\mathbf{k}',\,\nu} \int \frac{\mathrm{d}\omega'}{2\pi} \left| g_{\mathbf{k},\,\mathbf{k}'}^{\mathbf{k}-\mathbf{k}',\,\nu} \right|^2 D(\mathbf{k} - \mathbf{k}', \nu, \omega - \omega') G(\mathbf{k}', \omega') \,. \tag{9}$$

For later convenience we present the phonon function $D(\mathbf{k}, \nu, \omega)$ in the spectral form

$$D(\mathbf{k}, \nu, \omega) = \frac{1}{\pi} \int_0^{\infty} \mathrm{d}\Omega \, \mathrm{Im}\, D(\mathbf{k}, \nu, \Omega) \times \left(\frac{1}{\omega - \Omega + \mathrm{i}\delta} - \frac{1}{\omega + \Omega - \mathrm{i}\delta} \right) . \tag{10}$$

In the adiabatic approximation and without regard for the phonon – phonon interaction, $\mathrm{Im}\, D(\mathbf{k}, \nu, \omega)$ is expressed as

$$\mathrm{Im}\, D(\mathbf{k}, \nu, \omega) = \pi\delta(\omega - \omega_{\mathbf{k}\nu}) \,. \tag{11}$$

The summation over vectors $\mathbf{k}'$ is conveniently presented as

$$\sum_{\mathbf{k}} = \int_{-\infty}^{\infty} \mathrm{d}\varepsilon \sum_{\mathbf{k}} \delta(\varepsilon - \varepsilon_{\mathbf{k}}) \,. \tag{12}$$

Using the above notation, $\Sigma(\mathbf{k}, \omega)$ can be rewritten as

$$\Sigma(\mathbf{k}, \omega) = \frac{\mathrm{i}}{\pi} \int \mathrm{d}\varepsilon \sum_{\mathbf{k}', \nu} \left| g_{\mathbf{k}, \mathbf{k}'}^{\mathbf{k}-\mathbf{k}', \nu} \right|^2 \delta(\varepsilon - \varepsilon_{\mathbf{k}'}) \times \int \mathrm{d}\Omega \, \mathrm{Im}\, D(\mathbf{k} - \mathbf{k}', \nu, \Omega) \int \frac{\mathrm{d}\omega'}{2\pi} G(\mathbf{k}', \omega') \times \left(\frac{1}{\omega - \omega' - \Omega + \mathrm{i}\delta} - \frac{1}{\omega - \omega' + \Omega - \mathrm{i}\delta} \right) . \tag{13}$$

As it is seen from (13), the absolute value of $\Sigma(\mathbf{k}, \omega)$ is of order ω_{D}. It follows, as Migdal has shown, that the electron Green's function in (13) can be replaced by Green's function $G_0(\mathbf{k}, \omega)$ for noninteracting electrons. As a result, (13) takes on the form

$$\Sigma(\mathbf{k}, \omega) = \frac{\mathrm{i}}{\pi} \int \mathrm{d}\varepsilon \sum_{\mathbf{k}', \nu} \left| g_{\mathbf{k}, \mathbf{k}'}^{\mathbf{k}-\mathbf{k}', \nu} \right|^2 \delta(\varepsilon - \varepsilon_{\mathbf{k}'}) \times \int \mathrm{d}\Omega \, \mathrm{Im}\, D(\mathbf{k} - \mathbf{k}', \nu, \Omega) \int \frac{\mathrm{d}\omega'}{2\pi} \frac{1}{\omega' - \varepsilon - \mathrm{i}\delta} \times \left(\frac{1}{\omega - \omega' - \Omega + \mathrm{i}\delta} - \frac{1}{\omega - \omega' + \Omega - \mathrm{i}\delta} \right) . \tag{14}$$

The analysis of (14), as performed by Migdal, shows that the essential values of ω and ω' are of the order of ω_{D}. This means that small frequencies of the order of ω_{D} are also significant for ε. In this case ε can be neglected in $\delta(\varepsilon - \varepsilon_{\mathbf{k}})$. After that we integrate easily over ε and finally express $\Sigma(\mathbf{k}, \omega)$ as

$$\Sigma(\mathbf{k}, \omega) = \frac{1}{\pi} \int \mathrm{d}\Omega \sum_{\mathbf{k}', \nu} \left| g_{\mathbf{k}, \mathbf{k}'}^{\mathbf{k}-\mathbf{k}', \nu} \right|^2 \delta(\varepsilon_{\mathbf{k}'}) \, \mathrm{Im}\, D(\mathbf{k} - \mathbf{k}', \nu, \Omega) \times \int \mathrm{d}\omega' \left(\frac{1}{\omega - \omega' + \Omega - \mathrm{i}\delta} - \frac{1}{\omega - \omega' - \Omega + \mathrm{i}\delta} \right) . \tag{15}$$

Introducing the EPI spectral density $\alpha_{\mathbf{k}}^2(\Omega) F(\Omega)$ equal to

$$\alpha_{\mathbf{k}}^2(\Omega) F(\Omega) = \sum_{\mathbf{k}', \nu} \left| g_{\mathbf{k}, \mathbf{k}'}^{\mathbf{k}-\mathbf{k}', \nu} \right|^2 \delta(\varepsilon_{\mathbf{k}'}) \, \mathrm{Im}\, D(\mathbf{k} - \mathbf{k}', \nu, \Omega) \,, \tag{16}$$

we derive $\Sigma(\mathbf{k}, \omega)$ in the form

$$\Sigma(\mathbf{k}, \omega) = \frac{1}{\pi} \int \mathrm{d}\Omega \, \alpha_{\mathbf{k}}^2(\Omega) F(\Omega) L(\omega, \Omega) \,. \tag{17}$$

Here we placed

$$L(\omega, \Omega) = \int \mathrm{d}\omega' \left(\frac{1}{\omega - \omega' + \Omega - \mathrm{i}\delta} - \frac{1}{\omega - \omega' - \Omega + \mathrm{i}\delta} \right) . \tag{18}$$

Notice firstly that by virtue of the above approximations, which are valid when $\omega_{\mathrm{D}} \ll \varepsilon_{\mathrm{F}}$, the function $\Sigma(\mathbf{k}, \omega)$ depends only on the angular part of the vector $\mathbf{k}$ lying on the Fermi surface. Integral (18) can be easily calculated for function $L(\omega, \Omega)$, but we will not do it here. It is readily shown that the expression for self-energy $\Sigma(\mathbf{k}, \omega)$ has precisely the same form as formula (17) at any temperature [15]. The function $L(\omega, \Omega)$ at $T \neq 0$ is expressed as

$$L(\omega, \Omega) = -2\pi\mathrm{i} \left[n(\Omega) + \frac{1}{2} \right] + \Psi\left(\frac{1}{2} + \mathrm{i} \, \frac{\Omega - \omega}{2\pi T} \right) - \Psi\left(\frac{1}{2} - \mathrm{i} \, \frac{\Omega + \omega}{2\pi T} \right) , \tag{19}$$

where $\Psi(x)$ is the digamma function, $n(\Omega)$ is the Bose-distribution function. We can determine the function $\Sigma(\omega)$, which yields the self-energy averaged over the Fermi surface, as

$$\Sigma(\omega) = \frac{1}{N(\varepsilon_{\mathrm{F}})} \sum_{\mathbf{k}} \delta(\varepsilon_{\mathbf{k}}) \Sigma(\mathbf{k}, \omega) \,, \tag{20}$$

where $N(\varepsilon_{\mathrm{F}})$ is the density of electron states on the Fermi surface; then we arrive at

$$\Sigma(\omega) = \int \mathrm{d}\Omega \, \alpha^2(\Omega) F(\Omega) \left\{ -2\pi\mathrm{i} \left[n(\Omega) + \frac{1}{2} \right] + \Psi\left(\frac{1}{2} + \mathrm{i} \, \frac{\Omega - \omega}{2\pi T} \right) - \Psi\left(\frac{1}{2} - \mathrm{i} \, \frac{\Omega + \omega}{2\pi T} \right) \right\} . \tag{21}$$

The above-introduced function $\alpha^2(\Omega) F(\Omega)$ is usually referred to as the EPI spectral density or the Eliashberg function and has the form

$$\alpha^2(\Omega) F(\Omega) = \frac{1}{N(\varepsilon_{\mathrm{F}})} \sum_{\mathbf{k}, \mathbf{q}, \nu} \left| g_{\mathbf{k}+\mathbf{q}, \mathbf{k}}^{\mathbf{q}\nu} \right|^2 \delta(\Omega - \omega_{\mathbf{q}\nu}) \delta(\varepsilon_{\mathbf{k}}) \delta(\varepsilon_{\mathbf{k}+\mathbf{q}}) \,. \tag{22}$$

This function determines, in particular, superconducting properties in metals.

As noted above, the Fröhlich Hamiltonian, though being inappropriate for the calculation of exact phonon spectra in the general case, nevertheless is suitable for finding the phonon damping. To do this, one should calculate the imaginary part of the phonon self-energy $\Pi(\mathbf{q}, \nu, \omega)$. Similar calculations were performed by Allen in Ref. [16], where the phonon damping $\gamma_{\mathbf{q}, \nu}$ for a given energy $\omega_{\mathbf{q}, \nu}$ was shown to be

$$\gamma_{\mathbf{q}\nu} = 2\pi \omega_{\mathbf{q}\nu} \sum_{\mathbf{k}} \left| g_{\mathbf{k}+\mathbf{q}, \mathbf{k}}^{\mathbf{q}\nu} \right|^2 \delta(\varepsilon_{\mathbf{k}}) \delta(\varepsilon_{\mathbf{k}+\mathbf{q}}) \,. \tag{23}$$

Comparing formulas (22) and (23), we see that the Eliashberg function can be presented in terms of phonon damping as

$$\alpha^2(\Omega) F(\Omega) = \frac{1}{2\pi N(\varepsilon_{\mathrm{F}})} \sum_{\mathbf{q}, \nu} \frac{\gamma_{\mathbf{q}\nu}}{\omega_{\mathbf{q}\nu}} \, \delta(\Omega - \omega_{\mathbf{q}\nu}) \,. \tag{24}$$

The self-energy component $\Sigma(\omega)$ incorporates real and imaginary parts and it can be given in the form

$$\Sigma(\omega) = -\omega \lambda(\omega, T) - \frac{\mathrm{i}}{2\tau(\omega, T)} \,. \tag{25}$$

It is well known that the function $\lambda(\omega, T)$ characterizes renormalization of the electron mass conditioned by the electron – phonon interaction, while $\tau(\omega, T)$ is the electron lifetime. We can easily see it, having rewritten the expression

for Green's function in the form

$$G(\mathbf{k},\omega)=\left[\frac{m^*(\omega,T)}{m}\,\omega-\varepsilon_{\mathbf{k}}+\frac{\mathrm{i}}{2\tau(\omega,T)}\right]^{-1}, \tag{26}$$

which involves the notation

$$\frac{m^*(\omega,T)}{m}=1+\lambda(\omega,T)\,. \tag{27}$$

Here m is the mass of noninteracting band electrons. At $T=0$ and $\omega=0$ the function $\lambda(\omega,T)$ presents the electron – phonon coupling constant

$$\lambda=2\int_0^\infty\frac{\mathrm{d}\Omega}{\Omega}\,\alpha^2(\Omega)F(\Omega)\,. \tag{28}$$

The quasi-particle energy is determined by the pole of Green's function and we have

$$E_{\mathbf{k}}=\frac{m}{m^*(E_{\mathbf{k}},T)}\,\varepsilon_{\mathbf{k}}-\frac{\mathrm{i}}{2\tilde{\tau}(E_{\mathbf{k}},T)}\,, \tag{29}$$

where $\tilde{\tau}(\omega,T)=\tau(\omega,T)m^*(\omega,T)/m$. Clearly, well-defined quasi-particles exist only on condition

$$\frac{1}{2\tilde{\tau}(E_{\mathbf{k}},T)}\ll E_{\mathbf{k}}\,. \tag{30}$$

As we will see subsequently, this inequality is not valid in metals for rather a wide energy range near the Fermi surface. However expression (26) for the electron Green's function can be applied to the EPI systems in a wider range and holds true provided that the small parameter $\omega_{\mathrm{D}}/\varepsilon_{\mathrm{F}}$ prevails. The imaginary part of Green's function can be measured directly in experiments on photoemission with angular resolution [17].

Using the Fröhlich Hamiltonian, we can calculate the electric conductivity $\sigma(\omega)$ caused by EPI in metals. (A detailed review of appropriate calculation methods is given in Ref. [18].) To do this, one must find the electromagnetic kernel $K_{\mu\nu}(\omega)=4\pi\sigma_{\mu\nu}(\omega)/\omega$, where $\mu=x,y,z$. In metals with cubic lattice, which will be dealt with in this review, this tensor is reduced to the scalar $K(\omega)$. In the temperature Green's function method $K(\omega)$ is given by

$$K(\nu_m)=4\pi e^2T\sum_{\omega_n}\sum_{\mathbf{k},\mu}v^\mu_{\mathbf{k}}G_{\mathbf{k}}(\omega_n)G_{\mathbf{k}}(\omega_n+\nu_m)\times\Gamma^\mu_{\mathbf{k}}(\omega_n,\omega_n+\nu_m)\,. \tag{31}$$

Here $\nu_m=2\pi Tm$ and $\omega_n=\pi T(2n+1)$; $v^\mu_{\mathbf{k}}$ are the electron velocity components; $\Gamma^\mu_{\mathbf{k}}(\omega_n,\omega_n+\nu_m)$ is the vertex function, which, in turn, can be presented as the integral equation

$$\Gamma^\mu_{\mathbf{k}}(\omega_n,\omega_n+\nu_m)=v^\mu_{\mathbf{k}}+T\sum_{\omega'_n}\sum_{\mathbf{k}'}W(\mathbf{k},\mathbf{k}')G_{\mathbf{k}'}(\omega'_n)\times G_{\mathbf{k}'+\mathbf{k}}(\omega_n-\omega'_n)\Gamma^\mu_{\mathbf{k}'}(\omega'_n,\omega'_n+\nu_m)\,. \tag{32}$$

Here $W(\mathbf{k},\mathbf{k}')$ is the electron – phonon interaction energy

$$W(\mathbf{k},\mathbf{k}')=\sum_\nu\left|g^{\mathbf{k}-\mathbf{k}',\nu}_{\mathbf{k},\mathbf{k}'}\right|^2\frac{2\omega_{\mathbf{k}-\mathbf{k}'\nu}}{\omega^2_{\mathbf{k}-\mathbf{k}'\nu}-(\omega_n-\omega'_n)^2}\,. \tag{33}$$

The equation for the vertex function $\Gamma^\mu_{\mathbf{k}}(\omega_n,\omega_n+\nu_m)$ can be solved by a variational method, with the probe function for $\Gamma^\mu_{\mathbf{k}}(\omega_n,\omega_n+\nu_m)$ chosen in the form

$$\Gamma^\mu_{\mathbf{k}}(\omega_n,\omega_n+\nu_m)=v^\mu_{\mathbf{k}}f(\omega_n,\omega_n+\nu_m)\,. \tag{34}$$

Bearing in mind, as we did in considering the one-particle Green's function, that EPI is localized near the Fermi-surface where all the quantities, except for the one-particle Green's function, change only slightly, we arrive at the ultimate expression for electric conductivity $\sigma(\omega)$ in a form closely resembling the one-particle Green's function:

$$\sigma(\omega)=\frac{\omega^2_{\mathrm{p}}}{4\pi}\,\frac{1}{-\mathrm{i}\omega+\Sigma_{\mathrm{tr}}(\omega)}\,. \tag{35}$$

The function $\Sigma_{\mathrm{tr}}(\omega)$, by analogy with the self-energy part $\Sigma(\omega)$, can also be written in terms of renormalized mass and relaxation time:

$$\Sigma_{\mathrm{tr}}(\omega)=\mathrm{i}\omega\left[1-\frac{m^*_{\mathrm{tr}}(\omega,T)}{m}\right]+\frac{1}{\tau_{\mathrm{tr}}(\omega,T)}\,. \tag{36}$$

Broadly speaking, expressions for the transport renormalized mass and relaxation time differ from those given by formula (21). At $T=0$ the formulas for

$$\frac{m^*_{\mathrm{tr}}(\omega,T)}{m}\quad\text{and}\quad\frac{1}{\tau_{\mathrm{tr}}(\omega,T)}$$

were first obtained by Allen [19]. Subsequently they were extended to the case of finite temperatures [20, 21]. In the general case these formulas have the form

$$\Sigma_{\mathrm{tr}}(\omega)=-2\mathrm{i}\int_0^\infty\mathrm{d}\Omega\,\alpha^2_{\mathrm{tr}}(\Omega)F(\Omega)K\left(\frac{\omega}{2\pi T},\frac{\Omega}{2\pi T}\right), \tag{37}$$

where

$$K(x,y)=\frac{\mathrm{i}}{y}+\left\{\frac{y-x}{x}\left[\Psi(1-\mathrm{i}x+\mathrm{i}y)-\Psi(1+\mathrm{i}y)\right]\right\}-\{y\to-y\}\,. \tag{38}$$

In describing the transfer processes, particularly optical conductivity, one more EPI spectral density $\alpha^2_{\mathrm{tr}}(\Omega)F(\Omega)$ arises, which can be presented as

$$\alpha^2_{\mathrm{tr}}(\Omega)F(\Omega)=\alpha^2_{\mathrm{out}}(\Omega)F(\Omega)-\alpha^2_{\mathrm{in}}(\Omega)F(\Omega)\,, \tag{39}$$

where

$$\alpha^2_{\mathrm{out(in)}}(\Omega)F(\Omega)=\frac{1}{N(\varepsilon_{\mathrm{F}})\langle v^2_x\rangle}\sum_{\mathbf{k},\mathbf{k}',\nu}\left|g^{\mathbf{k}-\mathbf{k}',\nu}_{\mathbf{k},\mathbf{k}'}\right|^2v_x(k)v_x(k^{(\prime)})\times\delta(\omega-\omega_{\mathbf{k}-\mathbf{k}'\nu})\delta(\varepsilon_{\mathbf{k}})\delta(\varepsilon_{\mathbf{k}'})\,. \tag{40}$$

Here $\langle v^2_x\rangle$ is the averaged electron velocity squared on the Fermi surface. This quantity is closely related to the plasma frequency ω_{p} entering the equation for optical conductivity:

$$\omega^2_{\mathrm{p}}=4\pi e^2N(\varepsilon_{\mathrm{F}})\langle v^2_x\rangle\,. \tag{41}$$

To conclude this section, we will give for reference the Eliashberg equations describing superconducting properties in metals, omitting their derivation. These equations contain two functions: the order parameter $\Delta(\omega)$, and the renormalization function $Z(\omega)$. In a normal state $\Delta(\omega)$ is clearly equal

to zero, while the renormalization function $Z(\omega)$ transforms to the earlier introduced mass renormalization function $Z^{\mathrm{N}}(\omega, T) = m^*(\omega, T)/m$:

$$Z(\omega)\Delta(\omega) = \int_{-\infty}^{\infty} \mathrm{d}\omega' \,\mathrm{Re}\left\{\frac{\Delta(\omega')}{\left[\omega'^2 - \Delta^2(\omega')\right]^{1/2}}\right\}$$
$$\times \int_0^{\infty} \mathrm{d}\Omega\, \alpha^2(\Omega) F(\Omega) \left[\frac{f(-\omega') + n(\Omega)}{\omega' + \Omega - \omega} + \frac{f(\omega') + n(\Omega)}{\omega' - \Omega - \omega}\right]$$
$$- \mu(\varepsilon_{\mathrm{F}}) \int_0^{\varepsilon_{\mathrm{F}}} \mathrm{d}\omega' \,\mathrm{Re}\left\{\frac{\Delta(\omega')}{\left[\omega'^2 - \Delta^2(\omega')\right]^{1/2}}\right\} \tanh \frac{\omega'}{2T}\,, \quad (42)$$

$$\left[1 - Z(\omega)\right]\omega = \int_0^{\infty} \mathrm{d}\omega' \,\mathrm{Re}\left\{\frac{\omega'}{\left[\omega'^2 - \Delta^2(\omega')\right]^{1/2}}\right\}$$
$$\times \int_0^{\infty} \mathrm{d}\Omega\, \alpha^2(\Omega) F(\Omega) \left[\frac{f(-\omega') + n(\Omega)}{\omega' + \Omega + \omega} - \frac{f(-\omega') + n(\Omega)}{\omega' + \Omega - \omega}\right.$$
$$\left. + \frac{f(\omega') + n(\Omega)}{-\omega' + \Omega + \omega} - \frac{f(\omega') + n(\Omega)}{-\omega' + \Omega - \omega}\right]. \quad (43)$$

Here $f(\omega)$ is the Fermi distribution function, and $\mu(\varepsilon_{\mathrm{F}})$ is the averaged Coulomb interaction between electrons. Unfortunately, to date no reasonable methods for calculating $\mu(\varepsilon_{\mathrm{F}})$ have been developed and most commonly $\mu(\varepsilon_{\mathrm{F}})$ has been considered as a phenomenological constant.

3. Application of the Landau Fermi-liquid theory to the electron – phonon interaction

The EPI contribution to the one-particle electron Green's function can formally be calculated using the many-body perturbation theory for the total electron – ion (or, more precisely, electron-nucleus) Hamiltonian. Within this approach the EPI contribution to the self-energy part $\Sigma(x, x')$ can be written as [1, 22]

$$\Sigma_{\mathrm{ph}} = \int \Gamma_{\mathrm{e}} \boldsymbol{\nabla} \widetilde{V} D G \boldsymbol{\nabla} \widetilde{V} \Gamma_{\mathrm{e}}\,. \quad (44)$$

To avoid complicating this formula, we will not mark all the indices and only clarify the meaning of the notation used. Here G and D are the electron and phonon Green's functions, respectively, $\boldsymbol{\nabla}\widetilde{V}$ is the screened gradient of the electron – ion potential V_{ei}:

$$\boldsymbol{\nabla}\widetilde{V} = \sum_m \int \epsilon^{-1} \boldsymbol{\nabla} V_{\mathrm{ei}}(\mathbf{r} - \mathbf{R}_m)\,. \quad (45)$$

Here ϵ is the dielectric constant of the electron subsystem, such that

$$\epsilon = 1 + \int V_{\mathrm{C}} \Gamma_{\mathrm{e}} G G\,, \quad (46)$$

V_{C} is the Coulomb interelectron interaction, and $\Gamma_{\mathrm{e}} = \Gamma_{\mathrm{e}}(x_1, x_2, x_3)$ is the three-point vertex function determined, in turn, by a complicated integral equation.

A detailed analysis of (44) shows [1, 22] that the phonon contribution to the self-energy part formally coincides with that given by the Fröhlich Hamiltonian. The EPI matrix element presents rather a complicated expression involving a screened gradient of the bare Coulomb electron – ion potential and the vertex function of the Coulomb interelectron interaction. But, as was already noted, the EPI matrix element can be derived by another approach based on the theory of the Landau Fermi-liquid which we will present below. To start with, we will show that this approach yields precisely the same expression for the EPI matrix element as the conventional Green's function theory dealing with the total electron – ion Hamiltonian. Another aim of this approach is to determine a relationship between the exact expressions for the EPI matrix element and various approximations, widely used nowadays for numerical calculations.

It is well known that according to the Landau Fermi-liquid theory, the low-energy and low-temperature properties of strongly interacting Fermi particles can be described by weakly-interacting quasi-particles with a changed (due to the interaction) excitation spectrum [23]. In this case the total number of quasi-particles is equal to the total number of particles. The ideas of the Fermi-liquid theory were used in some papers (see, for example, Refs [24, 25]) to study the EPI effects. Essentially, this approach to the EPI theory is as follows. Since the EPI effects are significant only near the Fermi surface, assume that we have somehow determined the electron excitation energies, or equivalently — the Hamiltonian with full regard to the Coulomb interaction for an arbitrary ion arrangement. Suppose, it is $H(\mathbf{p}, \mathbf{r}, t, \{\mathbf{R}_n\})$, where $\mathbf{p}$ is the electron momentum, $\mathbf{r}$ its coordinate, t the time. This notation takes into account that the energy $H(\mathbf{p}, \mathbf{r}, t, \{\mathbf{R}_n\})$ is a functional of the ion arrangement $\{\mathbf{R}_n\}$. After that the function $H(\mathbf{p}, \mathbf{r}, t, \{\mathbf{R}_n\})$ can be expanded in small ion displacements $\mathbf{u}_n$ from the equilibrium position $\mathbf{R}_n^0$:

$$H(\mathbf{p}, \mathbf{r}, t, \{\mathbf{R}_n\}) = H_0(\mathbf{p}, t) + \sum_n \frac{\partial H}{\partial \mathbf{R}_n} \cdot \mathbf{u}_n\,. \quad (47)$$

The quantity $\partial H/\partial \mathbf{R}_n$ can be determined by various approximate methods such as the method of deformation potential. Knowing the Hamiltonian, we can write the kinetic equation for the electron distribution function and then evaluate the EPI influence on the physical properties of electrons, particularly on the electron transfer processes.

We will not dwell on the above-mentioned Fermi-liquid approach to EPI, but concentrate on the microscopic justification of the Landau Fermi-liquid theory. This analysis will enable, in particular, a more consistent formulation of the Fermi-liquid approach to EPI. To accomplish this, let us consider the one-particle Green's function $G(\mathbf{r}, \mathbf{r}', \omega)$ giving an insight into the quasi-particle excitation spectrum:

$$G^{-1}(\mathbf{r}, \mathbf{r}', \omega) = \omega + \frac{\nabla^2}{2m} - \sum_m V_{\mathrm{ei}}(\mathbf{r} - \mathbf{R}_m) - \Sigma(\mathbf{r}, \mathbf{r}', \omega) - \mu\,. \quad (48)$$

Here $\Sigma(\mathbf{r}, \mathbf{r}', \omega)$ is the self-energy part. In papers [26, 27] Luttinger and Ward introduced the functional Φ which enabled them to present $\Sigma(\mathbf{r}, \mathbf{r}', \omega)$ as

$$\Sigma(\mathbf{r}, \mathbf{r}', \omega) = \frac{\partial \Phi}{\partial G(\mathbf{r}, \mathbf{r}', \omega)}\,. \quad (49)$$

The same authors suggested a method for approximating the functional Φ in the framework of the self-consistent perturbation theory. The pertinent technique for a homogeneous electron gas was presented in a recent paper [28]. We will not discuss it in detail but restrict our consideration to the problems relevant for our further discussion.

Notice that the one-particle Green's function $G(\mathbf{r}, \mathbf{r}', \omega)$ cannot be diagonalized at finite ω in the representation of the Bloch wave functions, not even for a periodical lattice. We can, however, introduce a concept of an electron band structure, using Green's function $G(\mathbf{r}, \mathbf{r}', 0)$:

$$\left[-\frac{\nabla^2}{2m} + \sum_m V_{\mathrm{ei}}(\mathbf{r} - \mathbf{R}_m^0) + \mu\right] \Psi_{\mathbf{k}\lambda}(\mathbf{r}) + \int \mathrm{d}\mathbf{r}'\, \Sigma(\mathbf{r}, \mathbf{r}', 0) \Psi_{\mathbf{k}\lambda}(\mathbf{r}') = \varepsilon_{\mathbf{k}\lambda} \Psi_{\mathbf{k}\lambda}(\mathbf{r}) \,. \tag{50}$$

In Ref. [29], Eliashberg called this band structure kinematic and discussed some of its properties. We will outline them in what follows. On the one hand, as was noted by Luttinger [27], the band structure given by Eqn (50) determines the Fermi surface of a metal using the condition

$$\varepsilon_{\mathbf{k}_{\mathrm{F}}\lambda} = \mu \,, \tag{51}$$

where $\mathbf{k}_{\mathrm{F}}$ is the Fermi momentum at which the energy λ of electrons from the band intersects the level of the chemical potential. Another significant property of the band structure is that the so-called Luttinger theorem of equal numbers of particles and quasi-particles is valid:

$$\frac{N}{\Omega} = \frac{\partial \Phi}{\partial \mu} = \sum_{\mathbf{k}\lambda} f_{\mathbf{k}\lambda}(\varepsilon_{\mathbf{k}\lambda}) \,. \tag{52}$$

Here

$$f_{\mathbf{k}\lambda} = \begin{cases} 1 \,, & \varepsilon_{\mathbf{k}\lambda} \leqslant \mu \,, \\ 0 \,, & \varepsilon_{\mathbf{k}\lambda} > \mu \,. \end{cases} \tag{53}$$

Besides, the band structure is responsible for the density of electron states on the Fermi surface (and only on it!):

$$N(\varepsilon_{\mathrm{F}}) = -\frac{1}{\pi} \sum_{\mathbf{k}\lambda} \operatorname{Im} G(\mathbf{k}, \lambda, 0) = \sum_{\mathbf{k}\lambda} f_{\mathbf{k}\lambda} \delta(\varepsilon_{\mathbf{k}\lambda} - \mu) \,. \tag{54}$$

It should be emphasized that the corresponding electron band structure has never been evaluated for actual metal systems. The only exception is work [30], where it was numerically found for the one-dimensional Hubbard chain with ten points and was shown to possess a wide range of quite specific properties in strongly correlated systems. However, a detailed discussion of this problem is outside the scope of this review.

Notice that the band energy $\varepsilon_{\mathbf{k}\lambda}$ given by (50) does not determine the spectrum of quasi-particles even in proximity to the Fermi surface. The one-particle Green's function $G(\mathbf{k}, \lambda, \omega)$ at close range of the Fermi surface can be presented as [12, 31]

$$G(\mathbf{k}, \lambda, \omega) = \frac{Z_{\mathbf{k}\lambda}}{\omega - \tilde{\varepsilon}_{\mathbf{k}\lambda}} + f(\mathbf{k}, \lambda, \omega) \,, \tag{55}$$

where $f(\mathbf{k}, \lambda, \omega)$ is an incoherent part with no peculiarities near the Fermi surface. The excitation spectrum $\tilde{\varepsilon}_{\mathbf{k}\lambda}$ of quasi-particles in the neighbourhood of the Fermi surface has the form

$$\tilde{\varepsilon}_{\mathbf{k}\lambda} = Z_{\mathbf{k}\lambda} \varepsilon_{\mathbf{k}\lambda} \,. \tag{56}$$

The function $Z_{\mathbf{k}\lambda}$ characterizes a residue in Green's function pole and can be written as

$$\frac{1}{Z_{\mathbf{k}\lambda}} = 1 - \left\langle \Psi_{\mathbf{k}\lambda}(\mathbf{r}) \left| \frac{\partial \Sigma(\mathbf{r}, \mathbf{r}', \omega)}{\partial \omega} \right| \Psi_{\mathbf{k}\lambda}(\mathbf{r}') \right\rangle \Bigg|_{\omega = \tilde{\varepsilon}_{\mathbf{k}\lambda}} \,. \tag{57}$$

It was shown in the microscopic justification of the Landau Fermi-liquid theory [12, 31] that $Z_{\mathbf{k}\lambda}$ can be omitted due to the appropriate renormalization of effective interactions.

Now we will act in conformity with the spirit of the Landau Fermi-liquid theory and early papers on its application to the EPI theory. With this object in view we will introduce the Hamiltonian for electrons interacting with ions slightly displaced from the equilibrium position:

$$H = \sum_{\mathbf{k}\lambda} \left(\tilde{\varepsilon}_{\mathbf{k}\lambda} + Z_{\mathbf{k}\lambda} \sum_n \frac{\partial \tilde{\varepsilon}_{\mathbf{k}\lambda, \mathbf{k}'\lambda'}\{\mathbf{R}_n\}}{\partial \mathbf{R}_n} \cdot \mathbf{u}_n \right) , \tag{58}$$

where

$$\tilde{\varepsilon}_{\mathbf{k}\lambda, \mathbf{k}'\lambda'} = \left\langle \Psi_{\mathbf{k}\lambda}(\mathbf{r}) \middle| G^{-1}(\mathbf{r}, \mathbf{r}', 0) \middle| \Psi_{\mathbf{k}'\lambda'}(\mathbf{r}') \right\rangle . \tag{59}$$

Green's function $G(\mathbf{r}, \mathbf{r}', \omega)$ is defined by the following equation written in the operator form

$$\left[-\frac{\nabla^2}{2m} + \sum_m V_{\mathrm{ei}}(\mathbf{r} - \mathbf{R}_m) + \Sigma(\mathbf{r}, \mathbf{r}'', \omega)\right] G(\mathbf{r}'', \mathbf{r}, \omega) = \delta(\mathbf{r} - \mathbf{r}') \,, \tag{60}$$

$$\mathbf{R}_n = \mathbf{R}_n^0 + \mathbf{u}_n \,. \tag{61}$$

To find the exact Hamiltonian, we must calculate the function

$$\sum_n \left\langle \Psi_{\mathbf{k}\lambda}(\mathbf{r}) \left| \frac{\partial G^{-1}(\mathbf{r}, \mathbf{r}', 0)}{\partial \mathbf{R}_n} \right| \Psi_{\mathbf{k}'\lambda'}(\mathbf{r}') \right\rangle . \tag{62}$$

To this end, we will use equation (60) for Green's function and rewrite the self-energy part $\Sigma(\mathbf{r}, \mathbf{r}', \omega)$ in the form

$$\Sigma(\mathbf{r}, \mathbf{r}', \omega) = \Sigma_{\mathrm{H}}(\mathbf{r}) + \Sigma_{\mathrm{xc}}(\mathbf{r}, \mathbf{r}', \omega) \,. \tag{63}$$

Here $\Sigma_{\mathrm{H}}(\mathbf{r})$ stands for the Hartree contribution

$$\Sigma_{\mathrm{H}}(\mathbf{r}) = e^2 \int \frac{n(\mathbf{r}')}{|\mathbf{r} - \mathbf{r}'|} \, \mathrm{d}\mathbf{r}' \,, \tag{64}$$

$\Sigma_{\mathrm{xc}}(\mathbf{r}, \mathbf{r}', \omega)$ is the exchange-correlation contribution. Then (60) transforms to

$$\frac{\partial G^{-1}(\mathbf{r}, \mathbf{r}', 0)}{\partial \mathbf{R}_n} = \nabla V_{\mathrm{ei}}(\mathbf{r} - \mathbf{R}_n) + e^2 \int \frac{\mathrm{d}\mathbf{r}'}{|\mathbf{r} - \mathbf{r}'|} \frac{\partial n(\mathbf{r}')}{\partial \mathbf{R}_n} + \frac{\partial \Sigma_{\mathrm{xc}}(\mathbf{r}, \mathbf{r}', 0)}{\partial \mathbf{R}_n} \,. \tag{65}$$

According to the definition of electron susceptibility $\chi(\mathbf{r}, \mathbf{r}', \omega)$, we can write [22]

$$\frac{\partial n(\mathbf{r})}{\partial \mathbf{R}_n} = \int \mathrm{d}\mathbf{r}''\, \chi(\mathbf{r}, \mathbf{r}'', 0) \nabla V_{\mathrm{ei}}(\mathbf{r} - \mathbf{R}_n) \,. \tag{66}$$

Combining the first and the second terms in the right-hand side of Eqn (65), we have

$$\frac{\partial G^{-1}(\mathbf{r}, \mathbf{r}', 0)}{\partial \mathbf{R}_n} = \int \mathrm{d}\mathbf{r}''\, \epsilon^{-1}(\mathbf{r}, \mathbf{r}'', 0) \nabla V_{\mathrm{ei}}(\mathbf{r} - \mathbf{R}_n) + \int \mathrm{d}\mathbf{r}_1\, \mathrm{d}\mathbf{r}_2\, \mathrm{d}\omega\, \frac{\partial \Sigma_{\mathrm{xc}}(\mathbf{r}, \mathbf{r}', 0)}{\partial G(\mathbf{r}_1, \mathbf{r}_2, \omega)} \frac{\partial G(\mathbf{r}_1, \mathbf{r}_2, \omega)}{\partial \mathbf{R}_n} \,. \tag{67}$$

Here $\epsilon^{-1}(\mathbf{r},\mathbf{r}',0)$ is the inverse permittivity of the electron system, which equals, by definition,

$$\epsilon^{-1}(\mathbf{r},\mathbf{r}',0) = \delta(\mathbf{r}-\mathbf{r}') + e^2 \int \frac{\mathrm{d}\mathbf{r}''}{|\mathbf{r}-\mathbf{r}''|}\, \chi(\mathbf{r}'',\mathbf{r}',0)\,. \quad (68)$$

Using the identity

$$\frac{\partial G(\mathbf{r},\mathbf{r}',\omega)}{\partial \mathbf{R}_n} = -\int \mathrm{d}\mathbf{r}_1\, \mathrm{d}\mathbf{r}_2\, G(\mathbf{r},\mathbf{r}_1,\omega) \times \frac{\partial G^{-1}(\mathbf{r}_1,\mathbf{r}_2,\omega)}{\partial \mathbf{R}_n}\, G(\mathbf{r}_2,\mathbf{r}',\omega)\,, \quad (69)$$

we can write the ultimate equation to determine the function

$$\frac{\partial G^{-1}(\mathbf{r},\mathbf{r}',0)}{\partial \mathbf{R}_n}$$

in the form

$$\frac{\partial G^{-1}(\mathbf{r},\mathbf{r}',0)}{\partial \mathbf{R}_n} = \int \mathrm{d}\mathbf{r}''\, \epsilon^{-1}(\mathbf{r},\mathbf{r}'',0)\nabla V_{\mathrm{ei}}(\mathbf{r}-\mathbf{R}_n) - \int \mathrm{d}\mathbf{r}_1\, \mathrm{d}\mathbf{r}_2\, \mathrm{d}\mathbf{r}_3\, \mathrm{d}\mathbf{r}_4\, \mathrm{d}\omega\, \frac{\partial \Sigma_{\mathrm{xc}}(\mathbf{r},\mathbf{r}',0)}{\partial G(\mathbf{r}_1,\mathbf{r}_2,\omega)}\, G(\mathbf{r}_2,\mathbf{r}_3,\omega) \times \frac{\partial G^{-1}(\mathbf{r}_3,\mathbf{r}_4,\omega)}{\partial \mathbf{R}_n}\, G(\mathbf{r}_4,\mathbf{r}_2,\omega)\,. \quad (70)$$

This equation is easily solved by the previously introduced three-point vertex function $\Gamma(x,x',x_1)$, which can be presented in the coordinate space as

$$\Gamma(x,x',x_1) = \delta(x-x')\delta(x-x_1) + \int \mathrm{d}x_2\, \mathrm{d}x_3\, \mathrm{d}x_4\, \mathrm{d}x_5\, \frac{\partial \Sigma_{\mathrm{xc}}(x,x')}{\partial G(x_2,x_3)} \times G(x_2,x_4)\Gamma(x_4,x_5,x_1)G(x_5,x_3)\,. \quad (71)$$

As a result, we have

$$\frac{\partial G^{-1}(\mathbf{r},\mathbf{r}',0)}{\partial \mathbf{R}_n} = \int \mathrm{d}\mathbf{r}_1\, \mathrm{d}\mathbf{r}_2\, \Gamma(\mathbf{r},\mathbf{r}',\omega=0,\mathbf{r}_1) \times \epsilon^{-1}(\mathbf{r}_1,\mathbf{r}_2,0)\nabla V_{\mathrm{ei}}(\mathbf{r}_2-\mathbf{R}_n)\,. \quad (72)$$

Comparing the expression obtained for

$$\frac{\partial G^{-1}(\mathbf{r},\mathbf{r}',0)}{\partial \mathbf{R}_n}$$

with formula (44) for the self-energy part caused by EPI, we see that the EPI vertex function determined by the Fermi-liquid approach is precisely the same as that given by the many-body Green's function theory. Unfortunately, the EPI matrix element is unlikely to be calculated exactly at the moment. The inverse permittivity $\epsilon^{-1}(\mathbf{r},\mathbf{r}',0)$ and the electron vertex function $\Gamma(\mathbf{r},\mathbf{r}',\omega=0,\mathbf{r}_1)$ cannot be calculated on their own by the Fermi-liquid theory, since they are determined not only by properties of electrons on the Fermi surface, where, in fact, the theory applies, but also by properties of electrons away from the Fermi surface. Nevertheless, the Fermi-liquid approach as well as the many-body Green's function theory, provides reasons for using the Fröhlich Hamiltonian to describe the EPI influence on electron properties in metals both in normal and superconducting states. But it is possible only when the adiabatic parameter of the theory $\omega_{\mathrm{D}}/\varepsilon_{\mathrm{F}}$ is small. It should be reiterated that the EPI matrix element itself and the EPI spectral densities resulting from its adoption remain undefined material parameters of the system and should be calculated from some experimental data, for example, from the measurements of tunnelling spectra.

Recently, some success has been achieved in calculating Green's functions and vertex functions of a homogeneous electron gas [28]. This could enable the calculation of the properties of some simple metals with a weak electron-ion pseudopotential. However, little progress, if any, has been made in this direction. Most computations of the EPI matrix element performed to date have been based not on the many-body Green's function but on quite different approaches. In the next section we will dwell upon the technique of these calculations and discuss their validity for the problems where they are used as well as the limits of their applicability.

4. The density functional method and electron – phonon interaction

Most EPI calculations performed until now have been based on the density functional theory (DFT) which was first introduced by Hohenberg, Kohn, and Sham [7, 8] (for details see Ref. [9]). Essentially, the approach implies that the energy and other properties of the electron system in the ground state are a single-valued functional of the density distribution $n(\mathbf{r})$. The equilibrium density is given by the minimum of this functional

$$\frac{\delta E\{n(\mathbf{r})\}}{\delta n(\mathbf{r})} = 0\,. \quad (73)$$

Kohn and Sham [8] suggested defining the density of interacting electrons as that of some effective system of noninteracting electrons occurring in an effective field. In this case $n(\mathbf{r})$ can be represented as

$$n(\mathbf{r}) = \sum_{\mathbf{k}\lambda} f_{\mathbf{k}\lambda} \Psi^*_{\mathbf{k}\lambda}(\mathbf{r})\Psi_{\mathbf{k}\lambda}(\mathbf{r})\,, \quad (74)$$

where

$$f_{\mathbf{k}\lambda} = \begin{cases} 1\,, & \varepsilon_{\mathbf{k}\lambda} \leqslant \mu\,, \\ 0\,, & \varepsilon_{\mathbf{k}\lambda} > \mu\,. \end{cases} \quad (75)$$

The wave function of the effective system is described by the following Schrödinger equation (in this case usually referred to as the Kohn – Sham equation)

$$\left[-\frac{\nabla^2}{2m} + V_{\mathrm{eff}}(\mathbf{r})\right]\Psi_{\mathbf{k}\lambda}(\mathbf{r}) = \varepsilon_{\mathbf{k}\lambda}\Psi_{\mathbf{k}\lambda}(\mathbf{r})\,. \quad (76)$$

Here $V_{\mathrm{eff}}(\mathbf{r})$ is an effective potential defined as

$$V_{\mathrm{eff}}(\mathbf{r}) = \sum_n V_{\mathrm{ei}}(\mathbf{r}-\mathbf{R}_n) + V_{\mathrm{H}}(\mathbf{r}) + V_{\mathrm{xc}}(\mathbf{r})\,, \quad (77)$$

where $V_{\mathrm{H}}(\mathbf{r})$ is the Coulomb part of the Hartree potential of electrons, given by equation (64), $V_{\mathrm{xc}}(\mathbf{r})$ is the exchange – correlation potential

$$V_{\mathrm{xc}}(\mathbf{r}) = \frac{\delta E_{\mathrm{xc}}\{n(\mathbf{r})\}}{\delta n(\mathbf{r})}\,. \quad (78)$$

The exact exchange – correlation energy functional $E_{\rm xc}\{n(\mathbf{r})\}$ is, broadly speaking, unknown. In practice, the so-called local approximation is usually used for $E_{\rm xc}\{n(\mathbf{r})\}$ when employing the DFT:

$$E_{\rm xc}\{n(\mathbf{r})\} = \int n(\mathbf{r})\varepsilon_{\rm xc}\big(n(\mathbf{r})\big)\,\mathrm{d}\mathbf{r}\,. \tag{79}$$

Here $\varepsilon_{\rm xc}\big(n(\mathbf{r})\big)$ is the exchange-correlation energy per particle in a homogeneous electron gas with a given density $n = n(\mathbf{r})$. We will not discuss here all the advantages and disadvantages of the local approximation, for details the reader is referred to Refs [9, 32].

Formally the technique for calculating the EPI matrix element by the DFT is as follows. Suppose, the displacement $\mathbf{u}_n$ of ions from the equilibrium position $\mathbf{R}_n^0$ is specified. It results in the changed effective potential $V_{\rm eff}(\mathbf{r})$ in the Kohn – Sham equation:

$$V_{\rm eff}(\mathbf{r}) = V_{\rm eff}^0(\mathbf{r}) + \delta V_{\rm eff}(\mathbf{r})\,. \tag{80}$$

In this case $\delta V_{\rm eff}(\mathbf{r})$ can be represented as

$$\delta V_{\rm eff}(\mathbf{r}) = \sum_n \boldsymbol{\nabla} V_{\rm ei}(\mathbf{r}-\mathbf{R}_n^0)\cdot\mathbf{u}_n + \sum_n \frac{\delta V_{\rm H}(\mathbf{r})}{\delta\mathbf{R}_n}\cdot\mathbf{u}_n + \sum_n \frac{\delta V_{\rm xc}(\mathbf{r})}{\delta\mathbf{R}_n}\cdot\mathbf{u}_n\,. \tag{81}$$

Taking into account that $V_{\rm H}(\mathbf{r})$ and $V_{\rm xc}(\mathbf{r})$ depend on $n(\mathbf{r})$, Eqn (81) is rewritten in the form

$$\delta V_{\rm eff}(\mathbf{r}) = \sum_n \boldsymbol{\nabla} V_{\rm ei}(\mathbf{r}-\mathbf{R}_n^0)\cdot\mathbf{u}_n + \sum_n \int \mathrm{d}\mathbf{r}'\,\frac{\delta V_{\rm H}(\mathbf{r})}{\delta n(\mathbf{r}')}\,\frac{\delta n(\mathbf{r}')}{\delta\mathbf{R}_n}\cdot\mathbf{u}_n + \sum_n \int \mathrm{d}\mathbf{r}'\,\frac{\delta V_{\rm xc}(\mathbf{r})}{\delta n(\mathbf{r}')}\,\frac{\delta n(\mathbf{r}')}{\delta\mathbf{R}_n}\cdot\mathbf{u}_n\,. \tag{82}$$

Within the linear response theory $\delta n(\mathbf{r})/\delta\mathbf{R}_n$ can be given by the expression which was used earlier [see (66)]:

$$\frac{\delta n(\mathbf{r})}{\delta\mathbf{R}_n} = \int \mathrm{d}\mathbf{r}'\,\chi(\mathbf{r},\mathbf{r}')\boldsymbol{\nabla} V_{\rm ei}(\mathbf{r}'-\mathbf{R}_n)\,.$$

The DFT enables another form for $\delta n(\mathbf{r})/\delta\mathbf{R}_n$, viz.

$$\frac{\delta n(\mathbf{r})}{\delta\mathbf{R}_n} = \int \mathrm{d}\mathbf{r}'\,\chi_0(\mathbf{r},\mathbf{r}')\,\frac{\delta V_{\rm eff}(\mathbf{r}')}{\delta\mathbf{R}_n}\,, \tag{83}$$

where $\chi_0(\mathbf{r},\mathbf{r}')$ is the susceptibility of noninteracting electrons, described by the Kohn – Sham equation (76):

$$\chi_0(\mathbf{r},\mathbf{r}') = \sum_{\mathbf{k}\lambda,\lambda',\mathbf{q}} \frac{(f_{\mathbf{k}+\mathbf{q},\lambda'} - f_{\mathbf{k}\lambda})\Psi^*_{\mathbf{k}\lambda}(\mathbf{r})\Psi_{\mathbf{k}\lambda}(\mathbf{r}')\Psi^*_{\mathbf{k}+\mathbf{q}\lambda'}(\mathbf{r}')\Psi_{\mathbf{k}+\mathbf{q}\lambda'}(\mathbf{r})}{\varepsilon_{\mathbf{k}+\mathbf{q}\lambda'} - \varepsilon_{\mathbf{k}\lambda}}\,. \tag{84}$$

Using the above formulas, we can easily find the expression for $\delta V_{\rm eff}(\mathbf{r})/\delta\mathbf{R}_n$ which resembles closely the one obtained for $\delta G^{-1}(\mathbf{r},\mathbf{r}')/\delta\mathbf{R}_n$ in the previous section [see (72)]:

$$\frac{\delta V_{\rm eff}(\mathbf{r})}{\delta\mathbf{R}_n} = \int \mathrm{d}\mathbf{r}_1\,\mathrm{d}\mathbf{r}_2\,\widetilde{\Gamma}(\mathbf{r},\mathbf{r}_1)\epsilon^{-1}(\mathbf{r}_1,\mathbf{r}_2,0)\boldsymbol{\nabla} V_{\rm ei}(\mathbf{r}_2-\mathbf{R}_n) \tag{85}$$

where the vertex function $\widetilde{\Gamma}(\mathbf{r},\mathbf{r}_1)$ satisfies the equation

$$\widetilde{\Gamma}(\mathbf{r},\mathbf{r}_1) = \delta(\mathbf{r}-\mathbf{r}_1) + \int \mathrm{d}\mathbf{r}_2\,\mathrm{d}\mathbf{r}_3\,\frac{\delta V_{\rm xc}(\mathbf{r})}{\delta n(\mathbf{r}_2)}\,\chi_0(\mathbf{r}_2,\mathbf{r}_3)\widetilde{\Gamma}(\mathbf{r}_3,\mathbf{r}_1)\,. \tag{86}$$

The function $\epsilon^{-1}(\mathbf{r}_1,\mathbf{r}_2,0)$ is nothing but a standard inverse permittivity of the system coinciding with that introduced in the previous section, namely

$$\epsilon^{-1}(\mathbf{r},\mathbf{r}',0) = \delta(\mathbf{r}-\mathbf{r}') + e^2\int \mathrm{d}\mathbf{r}_1\,\frac{\chi(\mathbf{r}_1,\mathbf{r}',0)}{|\mathbf{r}-\mathbf{r}_1|}\,, \tag{87}$$

and $\chi(\mathbf{r},\mathbf{r}',0)$ is the susceptibility of the electron subsystem, given within the DFT by the equation

$$\chi(\mathbf{r},\mathbf{r}',0) = \chi_0(\mathbf{r},\mathbf{r}') + \int \mathrm{d}\mathbf{r}_1\,\mathrm{d}\mathbf{r}_2\left[\frac{e^2}{|\mathbf{r}-\mathbf{r}_1|} + \frac{\delta V_{\rm xc}(\mathbf{r})}{\delta n(\mathbf{r}_1)}\right]\chi_0(\mathbf{r}_1,\mathbf{r}_2)\chi(\mathbf{r}_2,\mathbf{r}')\,. \tag{88}$$

The expression for the change in the effective potential and, consequently, for the EPI matrix element obtained by the DFT significantly resembles that found earlier by the Fermi-liquid theory. At the same time, there are substantial discrepancies between these expressions. Let us begin with the pleasant point. As distinct from the Fermi-liquid theory, the effective potential change can be calculated completely by the DFT. The inverse static permittivity $\epsilon^{-1}(\mathbf{r}_1,\mathbf{r}_2,0)$ and the vertex function $\widetilde{\Gamma}(\mathbf{r}_1,\mathbf{r}_2)$ are found as solutions to (86), (88). Moreover, to get the function $\delta V_{\rm eff}(\mathbf{r})/\delta\mathbf{R}_n$, one need not calculate (by rather a complicated procedure) functions $\epsilon^{-1}(\mathbf{r}_1,\mathbf{r}_2,0)$ and $\widetilde{\Gamma}(\mathbf{r}_1,\mathbf{r}_2)$. The Sternheimer method [33] extended to crystals [34, 35] is suitable at this point. The essence of the method is as follows. Let us consider the Kohn – Sham equation (76) and specify the ion displacements $\mathbf{u}_n$. Then the equation transforms to

$$\left[-\frac{\nabla^2}{2m} + V_{\rm eff}^0(\mathbf{r}) + \sum_n \frac{\delta V_{\rm eff}(\mathbf{r})}{\delta\mathbf{R}_n}\cdot\mathbf{u}_n\right]\Psi_{\mathbf{k}\lambda}(\mathbf{r}) = \left(\varepsilon^0_{\mathbf{k}\lambda} + \sum_n \frac{\delta\varepsilon_{\mathbf{k}\lambda}}{\delta\mathbf{R}_n}\cdot\mathbf{u}_n\right)\Psi_{\mathbf{k}\lambda}(\mathbf{r})\,. \tag{89}$$

We will seek its solution in the form

$$\Psi_{\mathbf{k}\lambda}(\mathbf{r}) = \Psi^0_{\mathbf{k}\lambda}(\mathbf{r}) + \sum_n \frac{\delta\Psi_{\mathbf{k}\lambda}(\mathbf{r})}{\delta\mathbf{R}_n}\cdot\mathbf{u}_n\,. \tag{90}$$

Substituting the expression for $\Psi_{\mathbf{k}\lambda}(\mathbf{r})$ into (89) and collecting the first-order terms in $\mathbf{u}_n$, we arrive at the equation for $\Psi^0_{\mathbf{k}\lambda}(\mathbf{r})$ as well as that for the changing wave function:

$$\left[-\frac{\nabla^2}{2m} + V^0_{\rm eff}(\mathbf{r})\right]\frac{\delta\Psi_{\mathbf{k}\lambda}(\mathbf{r})}{\delta\mathbf{R}_n} = \left[\frac{\delta\varepsilon_{\mathbf{k}\lambda}}{\delta\mathbf{R}_n} - \frac{\delta V_{\rm eff}(\mathbf{r})}{\delta\mathbf{R}_n}\right]\Psi^0_{\mathbf{k}\lambda}(\mathbf{r})\,, \tag{91}$$

and $\delta V_{\rm eff}(\mathbf{r})/\delta\mathbf{R}_n$ is expressed by (82). According to the conventional rules of quantum mechanics, $\delta n(\mathbf{r})/\delta\mathbf{R}_n$ can be written as

$$\frac{\delta n(\mathbf{r})}{\delta\mathbf{R}_n} = \sum_{\mathbf{k}\lambda} f_{\mathbf{k}\lambda}\left[\Psi^{0*}_{\mathbf{k}\lambda}(\mathbf{r})\frac{\delta\Psi_{\mathbf{k}\lambda}(\mathbf{r})}{\delta\mathbf{R}_n} + \Psi^0_{\mathbf{k}\lambda}(\mathbf{r})\,\frac{\delta\Psi^*_{\mathbf{k}\lambda}(\mathbf{r})}{\delta\mathbf{R}_n}\right]\,. \tag{92}$$

Solving the initial Kohn-Sham equation for an ideal crystal in combination with equation (91) for changes in the wave

function, we can also find $\delta V_{\text{eff}}(\mathbf{r})/\delta \mathbf{R}_n$, using formulas (82) and (92). Moreover, as was detailed in Ref. [10], within the DFT we can calculate the dynamic matrix as well. It is expressed as

$$\frac{\partial^2 E_{\text{tot}}}{\partial \eta_{\mu\mathbf{q}} \partial \eta^*_{\mu'\mathbf{q}}} = \int \mathrm{d}\mathbf{r}\, \frac{\delta(n+n_{\text{ext}})}{\delta \eta_{\mu\mathbf{q}}} \frac{\delta V_{\text{ext}}}{\delta \eta^*_{\mu'\mathbf{q}}} + \int \mathrm{d}\mathbf{r}\, (n+n_{\text{ext}}) \frac{\delta^2 V_{\text{ext}}}{\delta \eta_{\mu\mathbf{q}} \delta \eta^*_{\mu'\mathbf{q}}} \tag{93}$$

within an accuracy of a multiplier related to nucleus mass. Here μ is the coordinate subscript, n_{ext} is the point charge density of nuclei. Thus, the DFT seemingly provides all the components necessary to calculate the EPI. The electron spectrum is given by Kohn – Sham equation (76). The phonon spectrum of a metal can be calculated from equation (93) for the dynamic matrix. Finally, equation (82) for the change in the effective potential enables the easy calculation of its matrix element using the wave functions $\Psi_{\mathbf{k}\lambda}(\mathbf{r})$ and $\Psi_{\mathbf{k}+\mathbf{q}\lambda'}(\mathbf{r})$. However, there is at least one substantial and unpleasant difference between the DFT and the Fermi-liquid theory in consideration of electron – phonon interactions. Suppose we have calculated changes in the effective potential within the DFT and found an appropriate matrix element, but we do not know how to treat it within this method. The point is that the conventional DFT only describes the properties of the ground state of the system. At the same time, electron transitions caused by EPI and defined by the corresponding matrix element are not determined by the ground state. They are associated with excited states of the system. As already noted, the DFT can be formally extended to nonequilibrium processes. However, no adequate procedure has been developed so far to do proper calculations on a coupled electron – phonon system.

Since the early attempts to compute the EPI matrix element by the DFT [6, 36, 37] the conventional approach to the problem has been as follows. The matrix element of the effective potential change has been found from the Kohn – Sham equation in the framework of the DFT. Then the result obtained has been used to calculate physical properties of metals using the conventional many-body theory based on the Fröhlich Hamiltonian. As was shown in the previous section, this approach is *a priori* appropriate within the Fermi-liquid theory. How far would the given approach with the use of the DFT be justified? Clearly, both the matrix elements coincide if the excitation spectra of the one-particle Green's function (50) and those of the DFT (76) do. The fact that in a general way these spectra differ is readily demonstrated by the example of a homogeneous interacting electron gas. The DFT yields in this case the spectrum of the form

$$\varepsilon_{\mathbf{k}} = \frac{k^2}{2m} - \mu\,, \tag{94}$$

where m is the free electron mass. At the same time, the excitation spectrum of the one-particle Green's function even close to the Fermi surface takes the form

$$\varepsilon_{\mathbf{k}} = \frac{k^2}{2m^*} - \mu\,, \tag{95}$$

where $m^* \neq m$. At least both the Fermi surfaces arising in Green's function method and in the DFT coincide in a homogeneous electron gas. But it is not generally the case. Thus in metals with a complicated Fermi surface not only the excitation spectra but both the Fermi surfaces can differ [32]. As is evident from considerable experimental data, the Fermi surface dissimilarities from that dictated by DFT and even the differences in the spectrum are insignificant for a number of metals [32], becoming noticeable in metals with strong exchange-correlation effects [30, 32, 38]. Unfortunately, this problem has not as yet been studied fully.

In this connection, direct and consistent calculations of EPI effects employing the DFT and their comparison with the experimental results seem all the more interesting. Many previous attempts to describe EPI in the framework of the DFT were rather inconsistent. In some of them only the electron contributions were calculated [6], while the phonon frequencies $\omega_{\mathbf{q}\nu}$ and eigenvectors $\mathbf{e}_{\mathbf{q}\nu}$ were fitted from experimental data on inelastic neutron scattering. Notice that the change in the effective potential was therewith determined by the rigid ion displacement approximation, i.e. $\nabla V_{\text{eff}}(\mathbf{r}-\mathbf{R}_n)$ was actually calculated. For isotropic metals with high density of states on the Fermi surface this approximation is valid in many cases, since due to strong screening the potential changes only near a displaced ion. However, in transition metals satisfying this criterion in many respects the above approximation of rigid ion displacement sometimes appears inadequate [37]. For example, it does not enable the description of anisotropic renormalization of the electron mass in Nb.

Recently an approach based on the linear response theory was developed [39], where a basis corresponding to the linear MT-orbital method (LMTO) [40] was used for the first-order correction to the wave function $\delta\Psi_{\mathbf{k}\lambda}(\mathbf{r})$. A substantial advantage of this method is that systems with narrow bands, such as d-bands, are considered in just the same way as wide-band systems without deterioration of the convergence. The method developed was used to calculate the phonon spectra of many metals [39, 41] (see also Ref. [10]) and to find EPI and its influence on the physical properties of metals [42, 43]. In the next section we will consider this method at length and present the calculated data on many properties of metals, determined by EPI.

5. The linear response theory and calculations of electron – phonon interactions in particular metals

The central problem in the calculation of the EPI matrix element and the dynamic matrix lies in determining $\delta V_{\text{eff}}/\delta\eta_{\mathbf{q}}$, where δV_{eff} is the change in the electron Hamiltonian, caused by the atom displacement

$$\mathbf{u}_n = \boldsymbol{\eta}_{\mathbf{q}} \exp(\mathrm{i}\mathbf{q}\cdot\mathbf{R}_n) + \boldsymbol{\eta}^*_{\mathbf{q}} \exp(-\mathrm{i}\mathbf{q}\cdot\mathbf{R}_n)\,.$$

As was detailed in our previous review [10], the calculation of $\delta V_{\text{eff}}/\delta\eta_{\mathbf{q}}$ is promoted by the fact that the change in the external potential $\delta V_{\text{ext}}/\delta\eta_{\mathbf{q}}$ transforms as the Bloch-like wave under $\mathbf{r}+\mathbf{R}_n$ augmentation. This means that if we know the change $\delta V_{\text{eff}}/\delta\eta_{\mathbf{q}}$ in one cell, we can easily calculate it for the whole crystal. Thus, equation (91) for changes in the wave function as well as the initial Kohn – Sham equation (76) for an unperturbed wave function should be solved only in one unit cell. The Kohn – Sham equation (76) with potential $V_{\text{eff}}(\mathbf{r})$ of arbitrary shape is usually solved through a variational principle. One constructs a functional and

minimizes it under the variation of one-electron functions, deriving as a result, the Schrödinger equation. In doing so the one-electron wave function is represented as an expansion in terms of a certain basis $\chi_n^{\mathbf{k}}(\mathbf{r})$:

$$\Psi_{\mathbf{k}\lambda}(\mathbf{r}) = \sum_n A_n^{\mathbf{k}\lambda} \chi_n^{\mathbf{k}}(\mathbf{r}) \,, \tag{96}$$

where $A_n^{\mathbf{k}\lambda}$ are the expansion coefficients, which display the variational parameters of the functional for the fixed basis $\chi_n^{\mathbf{k}}(\mathbf{r})$ and can be found as a solution to the matrix eigen-value problem

$$\sum_n \left\langle \chi_m^{\mathbf{k}} \middle| -\nabla^2 + V_{\text{eff}} - \varepsilon_{\mathbf{k}\lambda} \middle| \chi_n^{\mathbf{k}}(\mathbf{r}) \right\rangle A_n^{\mathbf{k}\lambda} = 0 \,. \tag{97}$$

According to the LMTO method, the crystal space is broken into nonoverlapping spheres centred on each atom (muffin-tin or MT-spheres) and the remaining interstitial regions. Within the MT-spheres the basis functions are linear combinations of numerical solutions to the Kohn – Sham radial equation, where the spherical part of the potential is employed, multiplied by spherical harmonics. This representation provides fast convergence of the basis for both delocalized and localized states. In the interstitial space where the potential is rather smooth, the basic functions are chosen as a solution to the Helmholtz equation $(-\nabla^2 - \kappa^2) f(\mathbf{r}) = 0$ for free electrons, where κ^2 is the electron kinetic energy in the interstitial space. In order to calculate EPI and phonon spectra, we should consider carefully the nonspherical contributions to the crystal potential, especially in the interstices, since vibrations of atoms in the direction towards each other significantly distort the electron density in this region. An approach to the solution of this problem was suggested in [41], where spherical harmonics were used in the MT-spheres as well as in the interstitial region. The crystal space was broken into polyhedral cells of Wigner – Seitz type, and MT-orbitals were represented as concentric expansions in terms of spherical harmonics up to the spheres around the polyhedrons. Such concentric expansions describe the electron density properly only in the atomic cell regions. Therefore, in order to solve the Poisson equation and calculate the matrix elements of the potential in the interspherical space, one should find an effective method for integrating functions over the region between the sphere and the polyhedron surface. The latter can be achieved by reducing the volume integrals to surface ones with the help of the Gauss theorem [41]. The advantage of this approach is the unified representation of all the quantities in terms of spherical harmonics for both the space regions. The processing rate of the method is only several times slower than that for the conventional LMTO method.

Let us consider the construction of linear MT-orbitals in more detail. The space is broken, in a way, into polyhedral cells of Wigner – Seitz type, circumscribing each atom. Inscribed MT-spheres and spheres circumscribing the polyhedra are introduced for these atomic cells. Both the spheres are centred at the lattice sites. Let us consider the so-called shell function. In the LMTO method this is the singular Hankel function $K_L(\mathbf{r}_t - \mathbf{R})$ centred at the site $\mathbf{R} + \mathbf{t}$ and determining the energy $\varepsilon = \kappa^2$. (Hereinafter we assume that all the radial functions involving vector notation in the parentheses are multiplied by spherical harmonics, L stands for the combined subscript lm, the subscript t on $\mathbf{r}$ means the difference $\mathbf{r} - \mathbf{t}$, where $\{\mathbf{t}\}$ are the positions of atoms in a unit cell, and $\{\mathbf{R}\}$ are the primitive translations.) Inside the self-sphere centred at $\mathbf{R} + \mathbf{t}$, the diverging part of the shell function is replaced by a linear combination of numerical radial functions smoothly joined onto the sphere boundary. Here the radial functions are the solutions $\phi_{tL}(\mathbf{r}_t - \mathbf{R}, \varepsilon_{vtl})$ to the Kohn – Sham equation taken with the spherical part of the potential and at certain energies ε_{vtl} from the range of interest, as well as their energy derivatives $\dot{\phi}_{tL}(\mathbf{r}_t - \mathbf{R}, \varepsilon_{vtl})$. Inside other atomic cells centred at $\mathbf{R}' + \mathbf{t}'$, the concentric expansion in terms of the Bessel functions is used for the tail of the shell function:

$$K_L(\mathbf{r}_t - \mathbf{R}) = \sum_{L'} J_{L'}(\mathbf{r}_{t'} - \mathbf{R}') S_{t'L'tL}(\mathbf{R}' - \mathbf{R}) \,, \tag{98}$$

where $J_L(\mathbf{r}_t - \mathbf{R})$ is the Bessel function, $S_{t'L'tL}(\mathbf{R})$ are structural constants in the direct space. Bearing in mind that Hankel and Bessel functions are given by the expressions

$$K_l(r) = -\frac{\mathrm{i}(\kappa w)^{l+1}}{(2l-1)!!} h_l(\kappa r) \,, \tag{99}$$

$$J_l(r) = \frac{1}{2} \frac{(2l-1)!!}{(\kappa w)^l} j_l(\kappa r) \,, \tag{100}$$

where $h_l = j_l - \mathrm{i} n_l$ are conventional Hankel spherical functions, and j_l, n_l are the Bessel and Neumann spherical functions, respectively, the expression for structural constants takes the form

$$S_{t'L'tL}(\mathbf{R}) = \sum_{L''} \frac{8\pi(2l''-1)!!}{(2l'-1)!!(2l-1)!!} C_{LL'}^{L''} (\kappa w)^{l+l'-l''} \times K_l\big(|\mathbf{R} - \mathbf{t}' + \mathbf{t}|\big)(-\mathrm{i})^{l''} Y_{L''}^*(\mathbf{R} - \mathbf{t}' + \mathbf{t}) \,, \tag{101}$$

where w is the average Wigner – Seitz radius, and $C_{LL'}^{L''}$ are the Gaunt coefficients. Finally, the linear MT-orbitals are obtained by substituting linear combinations of ϕ_{tL} and $\dot{\phi}_{tL}$ for the Bessel functions into all the MT-spheres, ϕ_{tL} and $\dot{\phi}_{tL}$ being chosen so that LMTO would be continuous and differentiable.

The final step is the summation over the grid of MT-orbitals centred at different lattice sites with the phase shift $\exp(\mathrm{i}\mathbf{k} \cdot \mathbf{R})$ so that the base functions would satisfy the Bloch theorem. It is easily obtained by summing only the structural constants (101), since now the orbitals constructed are everywhere the concentric expansions. As a result, the base functions are expressed as

$$\chi_{tL}^{\mathbf{k}}(\mathbf{r}_{t'}) = \Phi_{tL}^K(\mathbf{r}_t)\delta_{tt'} + \sum_{L'} \Phi_{t'L'}^J(\mathbf{r}_{t'}) S_{t'L'tL}^{\mathbf{k}} \quad \text{for} \quad r_{t'} < s_{t'} \,,$$

$$\chi_{tL}^{\mathbf{k}}(\mathbf{r}_{t'}) = K_{tL}(\mathbf{r}_t)\delta_{tt'} + \sum_{L'} J_{t'L'}(\mathbf{r}_{t'}) S_{t'L'tL}^{\mathbf{k}} \quad \text{for} \quad r_{t'} \in \Omega_{t'}^{\text{int}} \,, \tag{102}$$

where s_t are the radii of MT-spheres, and $S_{t'L'tL}^{\mathbf{k}}$ is the Fourier transform of structural constants (101):

$$S_{t'L'tL}^{\mathbf{k}} = \sum_{\mathbf{R}} \exp(\mathrm{i}\mathbf{k} \cdot \mathbf{R}) S_{t'L'tL}(\mathbf{R}) \,. \tag{103}$$

Here the radial functions $\Phi_{tL}^K(\mathbf{r}_t)$, $\Phi_{tL}^J(\mathbf{r}_t)$ are linear combinations of solutions ϕ_{tL} and $\dot{\phi}_{tL}$ smoothly joined with Hankel and Bessel functions on the sphere boundary.

Let us consider again the problem of the DFT linearization, characterizing the basis incompleteness. It results in high

errors for the atomic forces and dynamic matrix calculated by the exact density functional theory, in particular, by expression (93) for the dynamic matrix. The point is that in practice the wave functions are found not as an exact solution to the Kohn – Sham equation (76) but calculated approximately with the aid of the variational principle. In order to describe properly the changes in a wave function and related quantities under varied external parameters, the basis should be appropriate for the construction of the wave function with a certain accuracy over the whole range of the varied external parameters. Otherwise the derivative of the error could be large, which does happen in practice. In particular, the LMTO orbitals are centred at the sites of an unperturbed lattice and do not suit the description of wave functions in the presence of phonons. They must be reconstructed to include the specific atomic displacements. In other words, a reasonable dependence of the basis set on the displacement parameters is needed and some new terms $\mathrm{d}\chi_{tL}^{\mathbf{k}}/\mathrm{d}\mathbf{R}_t$ characterizing the changes in the basis due to the nucleus displacement $\mathbf{R}+\mathbf{t}=\mathbf{R}_t$ must be introduced into the expression for derivatives. In the LMTO method this dependence results immediately from the way of orbital construction. Considering the atomic coordinates as parameters rather than constants, we easily derive that the change in the basis set includes the 'rigid' orbital shift $-\delta\mathbf{R}_t\cdot\nabla\chi_{tL}^{\mathbf{k}}(\mathbf{r}_t)$ in each atomic cell plus the contribution given by the changed structural constants. The 'soft' part $\delta\chi_{tL}^{\mathbf{k}}$ associated with the $\delta^s\phi$ and $\delta^s\dot{\phi}$ variations is not taken into account. This contribution is rather small at a certain choice of parameters ε_v [10]. Thus, the alteration of the LMTO basis set is reduced to proper inclusion of the explicit dependence of an orbital on nucleus coordinates and can be easily calculated by differentiation of formulas (102) for MT-orbitals. Determining the atomic forces and the dynamic matrix at a fixed basis, we should bear in mind that the coefficients $A_\alpha^{\mathbf{k}\lambda}$ are only varied in the total energy functional presented by expansion (96) and the total energy shows an extremum under variation of these quantities only, so that the derivative $\mathrm{d}E/\mathrm{d}\mathbf{R}$ is defined by

$$\frac{\mathrm{d}E}{\mathrm{d}\{A_\alpha^{\mathbf{k}\lambda}\}}\,\frac{\mathrm{d}\{A_\alpha^{\mathbf{k}\lambda}\}}{\mathrm{d}\mathbf{R}}=0\,,$$

while contributions of the type

$$\frac{\mathrm{d}E}{\mathrm{d}\chi_{\kappa tL}^{\mathbf{k}}}\,\frac{\mathrm{d}\chi_{\kappa tL}^{\mathbf{k}}}{\mathrm{d}\mathbf{R}}\neq 0$$

are included as the so-called corrections for the basis set incompleteness.

Now let us turn to equation (91) governing the change in the effective one-particle potential. The matrix analog of this equation is the matrix Schrödinger equation (97), with the parametric dependence of the basis set taken into account. Varying successively all the quantities of the matrix equation (97) in the presence of the phonon $\mathbf{u}_{\mathbf{q}}$, we have

$$\begin{aligned}\sum_\alpha^N\Big\langle\chi_\beta^{\mathbf{k}+\mathbf{q}}\big|-\nabla^2+V_{\mathrm{eff}}-\varepsilon_{\mathbf{k}\lambda}\big|\chi_\alpha^{\mathbf{k}+\mathbf{q}}\Big\rangle\delta^{\mathbf{q}}A_\alpha^{\mathbf{k}\lambda}\\+\sum_\alpha^N\Big[\Big\langle\chi_\beta^{\mathbf{k}+\mathbf{q}}\big|\delta^{\mathbf{q}}V_{\mathrm{eff}}\big|\chi_\alpha^{\mathbf{k}}\Big\rangle+\Big\langle\delta^{\mathbf{q}}\chi_\beta^{\mathbf{k}-\mathbf{q}}\big|-\nabla^2+V_{\mathrm{eff}}-\varepsilon_{\mathbf{k}\lambda}\big|\chi_\alpha^{\mathbf{k}}\Big\rangle\\+\Big\langle\chi_\beta^{\mathbf{k}+\mathbf{q}}\big|-\nabla^2+V_{\mathrm{eff}}-\varepsilon_{\mathbf{k}\lambda}\big|\delta^{\mathbf{q}}\chi_\alpha^{\mathbf{k}}\Big\rangle\Big]A_\alpha^{\mathbf{k}\lambda}=0\,.\end{aligned}\tag{104}$$

The last two terms are associated with the variation of the basis set and represent the additional perturbation responsible for a change in the wave function

$$\delta^{\mathbf{q}}\Psi_{\mathbf{k}\lambda}(\mathbf{r})=\sum_n\big\{\delta^{\mathbf{q}}A_n^{\mathbf{k}\lambda}\chi_n^{\mathbf{k}}(\mathbf{r})+A_n^{\mathbf{k}\lambda}\delta^{\mathbf{q}}\chi_n^{\mathbf{k}}(\mathbf{r})\big\}\,.\tag{105}$$

This raises the question of what is meant by the matrix element of the electron – phonon interaction and how the correction for the basis set incompleteness shows up in this quantity. The simplest way to understand it is to consider the definition of the EPI spectral function (24) in terms of phonon linewidths (23). The phonon linewidth is determined by the Fermi 'golden rule', which describes the rate of transition of the initial unperturbed wave function $\Psi_{\mathbf{k}\lambda}$ into the final perturbed state $\widetilde{\Psi}_{\mathbf{k}\lambda}$ and follows from the analysis of the overlapping integral squared

$$\big|\langle\Psi_{\mathbf{k}\lambda}|\widetilde{\Psi}_{\mathbf{k}\lambda}\rangle\big|^2\,.$$

Since the final state corresponds to the disturbed lattice, the best variational estimate will be obtained with the basis, whose orbitals are centred at new atomic positions and include the peculiarities of the perturbing potential. Repeating the standard quantum-mechanical derivation of (23) for the finite space of probe functions $\{\chi_n\}$ depending on displacements, we easily find the EPI matrix element in the form

$$\begin{aligned}g_{\mathbf{k}+\mathbf{q}\lambda',\mathbf{k}\lambda}^{\mathbf{q}\nu}&=\big\langle\Psi_{\mathbf{k}+\mathbf{q}\lambda'}\big|\delta^{\mathbf{q}\nu}V_{\mathrm{eff}}\big|\Psi_{\mathbf{k}\lambda}\big\rangle\\&+\Big\langle\sum_n\delta^{\mathbf{q}\nu}\chi_n^{\mathbf{k}-\mathbf{q}}A_n^{\mathbf{k}+\mathbf{q}\lambda'}\big|-\nabla^2+V_{\mathrm{eff}}-\varepsilon_{\mathbf{k}\lambda}\big|\Psi_{\mathbf{k}\lambda}\Big\rangle\\&+\Big\langle\Psi_{\mathbf{k}+\mathbf{q}\lambda'}\big|-\nabla^2+V_{\mathrm{eff}}-\varepsilon_{\mathbf{k}+\mathbf{q}\lambda'}\big|\sum_n\delta^{\mathbf{q}\nu}\chi_n^{\mathbf{k}}A_n^{\mathbf{k}\lambda}\Big\rangle\,.\end{aligned}\tag{106}$$

Thus, the EPI matrix element must take into account the total perturbation responsible for the change in the wave function in Eqn (104), including the terms resulted from the basis set variation.

Now let us consider the numerical results produced in the framework of the above approach, which takes into account all the peculiarities discussed.

The band structure of Fcc metals such as Al, Cu, Pb, and Pd as well as that of Bcc metals including Mo, Nb, Ta, and V was calculated in an unperturbed lattice at 256 **k**-points of the Brillouin zone with the help of the spd-LMTO basis set at two different energies κ^2 for the tails of wave functions. Spherical harmonics up to $l_{\max}=8$ were used for the concentric expansion of the wave function and the potential. The same basis set was chosen to calculate the phonon frequencies $\omega_{\mathbf{q}\nu}$ in Al, Nb and Mo metals by the linear response theory. The phonon frequencies proved to be rather sensitive to the quality of the basis set, which motivated the choice of the above parameters for the LMTO-basis. Fortunately, $\omega_{\mathbf{q}\nu}$ is a relatively smooth function of **q** and can be calculated on a rather rough **q**-grid. The dynamic matrix was computed at 10 irreducible **q**-points of the Brillouin zone, then the former was transformed to the direct space: summing over **q**-points with factor $\exp(\mathrm{i}\mathbf{q}\cdot\mathbf{T})$, we constructed a dynamic matrix on the **T** grid in the direct space. Using the inverse Fourier transform and diagonalizing the dynamic matrix, we obtained the phonon fundamental frequencies and vectors for any **q**-point. Initially, we used experimental values of force constants to find phonon frequencies and vectors in Pb, V, Ta,

Pd, and Cu metals (see Ref. [44], Table 13a), since the procedure of the lattice dynamics calculation is time and labour consuming. Subsequently the lattice dynamics of these metals was examined theoretically with the help of the improved full-potential LMTO method, using a planar wave function in the intersphere space [43]. The results of all the calculations practically coincide, but in the current review we use the earliest ones. Necessary comments concerned with possible correction of the data presented will be made in what follows.

A few words must be said of the lattice parameters used in the calculations. It is well-known that the equilibrium volume calculated by the local density functional theory is somewhat less than the experimental one. As a consequence, the phonon frequencies calculated from the experimental lattice parameter are somewhat less than those observed. The theoretical lattice parameter often provides better agreement between the phonon spectra involved. In principle, this procedure is theoretically justified. However the calculated phonon linewidths and EPI spectral functions do not show a very good fit to the experimental data. The reason is that these quantities are rather sensitive to the shape of the Fermi surface. It turned out that the use of the Fermi surface calculated from the experimental lattice parameter significantly improved the agreement. Therefore, the lattice dynamics and the EPI matrix element were calculated with the aid of the theoretical lattice parameters, while the electron band structure involved in the definition of phonon linewidths and EPI spectral functions were computed from the experimental lattice parameter.

As distinct from $\omega_{\mathbf{q}\nu}$, the self-consistent screened potential $\delta V_{\mathbf{q}\nu}$ is less sensitive to the basis set. However, to integrate properly one must know it for a great deal of points from the Brillouin zone. We calculated the phonon linewidths $\gamma_{\mathbf{q}\nu}$ (24) at 47 $\mathbf{q}$-points. The potential $\delta V_{\mathbf{q}\nu}$ was calculated at each point, using a simpler basis set (47 $\mathbf{k}$-points instead of 256 and one energy κ^2 for the tails of the LMTO-basis functions), which increased the error only by $1-2\%$. Integration in (24) over the $\mathbf{k}$-space involved two δ-functions and was taken over a great number (752) of $\mathbf{k}$-points by the full-band method of tetrahedrons [45]. Data on $\gamma_{\mathbf{q}\nu}$ in Nb and Al metals, calculated along high-symmetrical directions are listed in Table 1. Similar results were obtained for Nb within the approximation of the MT-potential rigid shift (RMTA). They are in full agreement with data of Refs [46, 47] and confirm by the example of Al the earlier conclusion that approximations of this type are invalid for sp-metals. For reference, Table 1 lists experimental data on phonon linewidths for Nb [46]. These data correlate within experimental and calculation errors. Unfortunately, the experimental error is so large that no decisive inference can be made from this correlation. Our results obtained for Al correlated in general with the data found by the method of 'frozen' phonons with supercells [49] except that our result for the [110] longitudinal mode twice exceeded the data given in Ref. [49]. This discrepancy can be explained by different integration method used in Ref. [49], where δ functions were replaced by the corresponding Gaussian functions in (23). However, the relative contribution of γ into the integral values is very small.

Since phonon linewidths change significantly under variation of the wave vector, summation of $\alpha^2 F(\omega)$ over $\mathbf{q}$ in (24) should be performed on a rather dense grid. As was mentioned above, we used 47 $\mathbf{q}$-points and the maximal numerical error in $\alpha^2 F(\omega)$ resulted from the integration in $\mathbf{q}$-space. We estimated the error to be about 6%, having integrated phonon and electron δ-functions only (i.e. having put $\omega_{\mathbf{q}\nu}|g^{\mathbf{q}\nu}_{\mathbf{k}+\mathbf{q}\lambda',\mathbf{k}\lambda}|^2 = \text{const}$) at 47 and 752 $\mathbf{q}$-points, respectively. Thus, the total numerical error is estimated to be close to 10%. The function $\alpha^2 F(\omega)$ thus obtained for Al is shown in Fig. 1a (solid line). The positions of the maxima are determined by the shape of the phonon state density, the low-energy peak being suppressed by the coupling function α^2 (dashed line). The width of the phonon spectrum in Al metal is characterized by the maximum frequency $\omega_{\max} \approx 470$ K. As was noted in the previous section, the data calculated for Al by the method of 'frozen' phonons [49] correlate well with our results, and despite some discrepancy in the data on phonon linewidths, the curves for the EPI spectral density obtained by both the methods practically coincide.

The qualitative agreement of our curves with the tunnelling data on Pb is illustrated in Fig. 1b . A small discrepancy in the positions of the low maxima and additional theoretical peaks arising between the maxima in Pb are associated with the drawbacks of our calculation of the phonon spectrum. The tunnelling data better correspond to the observed density of phonon states. The errors in the calculation of Pb lattice dynamics result in overestimated frequencies of the transverse phonon mode near the band boundary at point X. This drawback does not fit into those discussed earlier in connection with the necessity of using different equilibrium volumes, since the experimental lattice parameter in Pb is correctly reproduced. It is not associated with the description

Table 1. Phonon linewidths γ_{L} and γ_{T} for longitudinal and transverse modes in Nb and Al metals in comparison with calculations in the rigid shift approximation (RMTA) and experimental data [46].

Nb$(\xi,\xi,0)$	$\xi = 0.1$	$\xi = 0.2$	$\xi = 0.3$	$\xi = 0.4$	$\xi = 0.5$
γ_{L}	0.133	0.180	0.279	0.404	0.370
$\gamma_{\mathrm{L}}^{\mathrm{RMTA}}$	0.091	0.138	0.291	0.485	0.444
$\gamma_{\mathrm{L}}^{\mathrm{exp}}$	0.13±0.05	0.21±0.05	0.31±0.06	0.48±0.09	0.43±0.13
γ_{T1}; γ_{T2}	0.019; 0.021	0.043; 0.032	0.057; 0.043	0.067; 0.068	0.109; 0.122
$\gamma_{\mathrm{T1}}^{\mathrm{RMTA}}$; $\gamma_{\mathrm{T2}}^{\mathrm{RMTA}}$	0.014; 0.021	0.037; 0.027	0.053; 0.053	0.070; 0.116	0.127; 0.211
$\gamma_{\mathrm{T}}^{\mathrm{exp}}$	0.02±0.02	0.06±0.04	0.12±0.04	0.11±0.06	—
Al$(\xi,0,0)$	$\xi = 0.2$	$\xi = 0.4$	$\xi = 0.6$	$\xi = 0.8$	$\xi = 1.0$
γ_{L}	0.039	0.072	0.095	0.112	0.071
$\gamma_{\mathrm{L}}^{\mathrm{RMTA}}$	0.012	0.012	0.014	0.018	0.012
γ_{T}	0.007	0.032	0.021	0.023	0.024
$\gamma_{\mathrm{T}}^{\mathrm{RMTA}}$	0.006	0.020	0.010	0.010	0.011

of the core states either, since 5d-states were considered in our calculation as energy bands rather than as atomic levels. Drawbacks of this sort in the calculation of the Pb phonon spectrum were noted earlier in Ref. [51], where the pseudopotential method was used within the linear response theory. Besides the error traditionally referred to the local density functional approximation, the anharmonism effects can also be mentioned as a possible reason of the discrepancy between the theoretical and experimental data on the Pb lattice dynamics.

V and Mo metals also possess rather a wide phonon spectrum (Fig. 1c, f) with $\omega_{\max} \simeq 370$ K and 390 K, respectively. The coupling function α^2 in these metals differs slightly from the constant over a wide range of the spectrum. The approximation $\alpha^2 = \text{const}$ is especially valid for Nb (Fig. 1d) and Ta (Fig. 1e). This qualitative result enables us to factorize the electron – phonon coupling constant in multipliers each depending on electron and phonon quantities only [52]. The latter are characterized by frequency moments determined solely by the spectrum of phonons, which have been studied much better than electrons. The calculated mean square of the phonon frequency in Ta $\langle\omega^2\rangle^{1/2} = 170$ K exceeds the value ~ 145 K obtained in the tunnelling experiments [50] by approximately 20%. Bearing in mind that frequency moments are mainly determined by the phonon spectrum, this 20% discrepancy can be assigned to drawbacks of the tunnelling data (where the high-frequency phonon peak can be underestimated) rather than to errors in theoretical considerations. The experimental function $\alpha^2 F(\omega)$ is found from tunnelling spectra by inversion of the Eliashberg equation and depends strongly on the method of handling the tunnelling data. Qualitative agreement between the obtained curves and tunnelling data for transition metals is readily seen in Fig. 1c, d, e. This agreement is not surprising since, as indicated above, the function $\alpha^2 F(\omega)$ is close in shape to the calculated density of phonon states. Aside from the value λ itself, the main difference between the theoretical and experimental curves for Nb and Va is in the peak heights. Assuming that $\alpha^2 = \text{const}$ is really valid in this case, we may conclude that the shape of the theoretical EPI function is more correct, since it merely reproduces the phonon density of states observed in experiments.

The most important characteristics pertinent to the EPI spectral density and its physical effects is the inverse frequency moment of the spectral function, or the electron – phonon coupling constant λ (28). Experimental values of this quantity can be immediately found from the EPI spectral functions restored from tunnelling data. On the other hand, according to definition (27) the electron – phonon coupling constant determines the EPI-caused renormalization of the electron mass. The change in the electron heat capacity given by the expression

$$1 + \lambda_{\mathrm{SH}} = \frac{3\gamma}{2\pi^2 k_{\mathrm{B}} N(\varepsilon_{\mathrm{F}})} \tag{107}$$

is a manifestation of this relation. Here γ is the linear coefficient in the temperature dependence of the electron heat capacity. The notation λ_{SH} is introduced to emphasize that this quantity relates to the phenomena associated with electron heat capacity. Now we will discuss the theoretical evaluations of the electron – phonon coupling constant λ as compared with estimations of λ_{tun} based on tunnelling data and values of λ_{SH} calculated by formula (107) with the use of experimental coefficient γ and our findings as regards the band computations of the phonon density of states $N(\varepsilon_{\mathrm{F}})$. All the data are listed in Table 2.

Table 2. Calculated EPI constants λ_{calc}, the tunnel-based estimations λ_{tun} [50, 53 – 55], and λ_{SH} found from the experimental linear coefficient γ [56, 57] entering the temperature dependence of electron heat capacity, with the use of calculated data on the phonon density of states $N(\varepsilon_{\mathrm{F}})$ [values of $N(\varepsilon_{\mathrm{F}})$ are given per atom allowing for spin degeneracy].

Parameter	Al	Pb	V	Nb	Ta	Mo	Cu	Pd
λ_{calc}	0.44	1.68	1.18	1.24	0.85	0.49	0.19	0.35
λ_{tun}	0.42	1.55	0.82	0.92; 1.22	0.78	—	—	—
λ_{SH}	0.43	1.64	1.17	1.16	0.83	0.45	—	0.69
$N(\varepsilon_{\mathrm{F}})$, Ry^{-1}	5.49	6.87	26.14	20.42	18.38	8.34	4.36	34.14
γ, mJ/(K^2 mol)	1.36	3.14	9.82	7.66	5.84	2.10	0.69	10.0

Tunnelling experiments on Al estimate the coupling constant as $\lambda_{\mathrm{tun}} = 0.42$, which is very close to our value $\lambda = 0.44$. The calculations by the method of 'frozen' phonons [49] and by earlier versions of the linear response theory [48] yield $\lambda = 0.45$ and $\lambda = 0.38$, respectively. To verify the assumption of the inapplicability of the RMTA-type approximation in sp-metals, we used this approximation in our calculations and indeed found $\lambda_{\mathrm{RMTA}} = 0.14$. Thus, the screening effects arising in the EPI effective potential are of considerable importance in sp-systems. Therefore, theoretical calculations taking proper account of these effects give similar results for the coupling constant close to the experimental data. Besides λ_{tun}, the value of $\lambda_{\mathrm{SH}} = 0.43$ calculated using formula (107) can serve as an experimental estimation. The experimental coefficient γ and the theoretical density of states $N(\varepsilon_{\mathrm{F}})$ are listed in Table 2. Another example to support the suitability of the EPI theory for sp-metals is Pb. The choice of this metal was motivated by the fact that it was thoroughly studied experimentally due to its rather high superconducting transition temperature $T_{\mathrm{c}} = 7.19$ K. The calculated value $\lambda = 1.68$ for Pb turned out to exceed the available estimate $\lambda_{\mathrm{tun}} = 1.55$ by 8% and $\lambda_{\mathrm{SH}} = 1.64$ by only 2%, the latter value being obtained from the measurements of the electron heat capacity (Table 2). Thus, within the numerical error of our calculations the theoretical and experimental data for Pb are also in complete agreement.

Now let us pass on to transition metals. Of most interest are V, Nb, and Ta which have long been studied by tunnelling methods due to their rather high critical temperatures (especially in Nb where $T_{\mathrm{c}} = 9.25$ K). The main problems in the study of Nb and V by the tunnelling spectroscopy are associated with oxidation processes in surface layers. The resultant oxides possess lower critical temperatures and distort the tunnelling spectrum due to the proximity effect. Tunnelling estimates of the coupling constant in Nb fall in the broad range from abnormally low values 0.58 – 0.68 [58, 59] to 0.9 [60]. So a wide variety of results can be attributed to the fact that in some early experiments the role of surface effects was not taken into consideration. Proper account of the proximity effects yields the estimate $\lambda_{\mathrm{tun}} = 0.92 - 1.22$ [54]. The same is true of V metal. High chemical activity of this metal hampers its study by tunnelling methods. The calculated EPI coupling constant of V exceeds by approximately 40% the available tunnelling estimate $\lambda_{\mathrm{tun}} = 0.82 \pm 0.05$ [55]. A similar situation holds for Nb, if setting $\lambda_{\mathrm{tun}} = 0.9$, as is customary. Of special interest in this respect is Ta. Having superconducting properties closely similar to those of V and

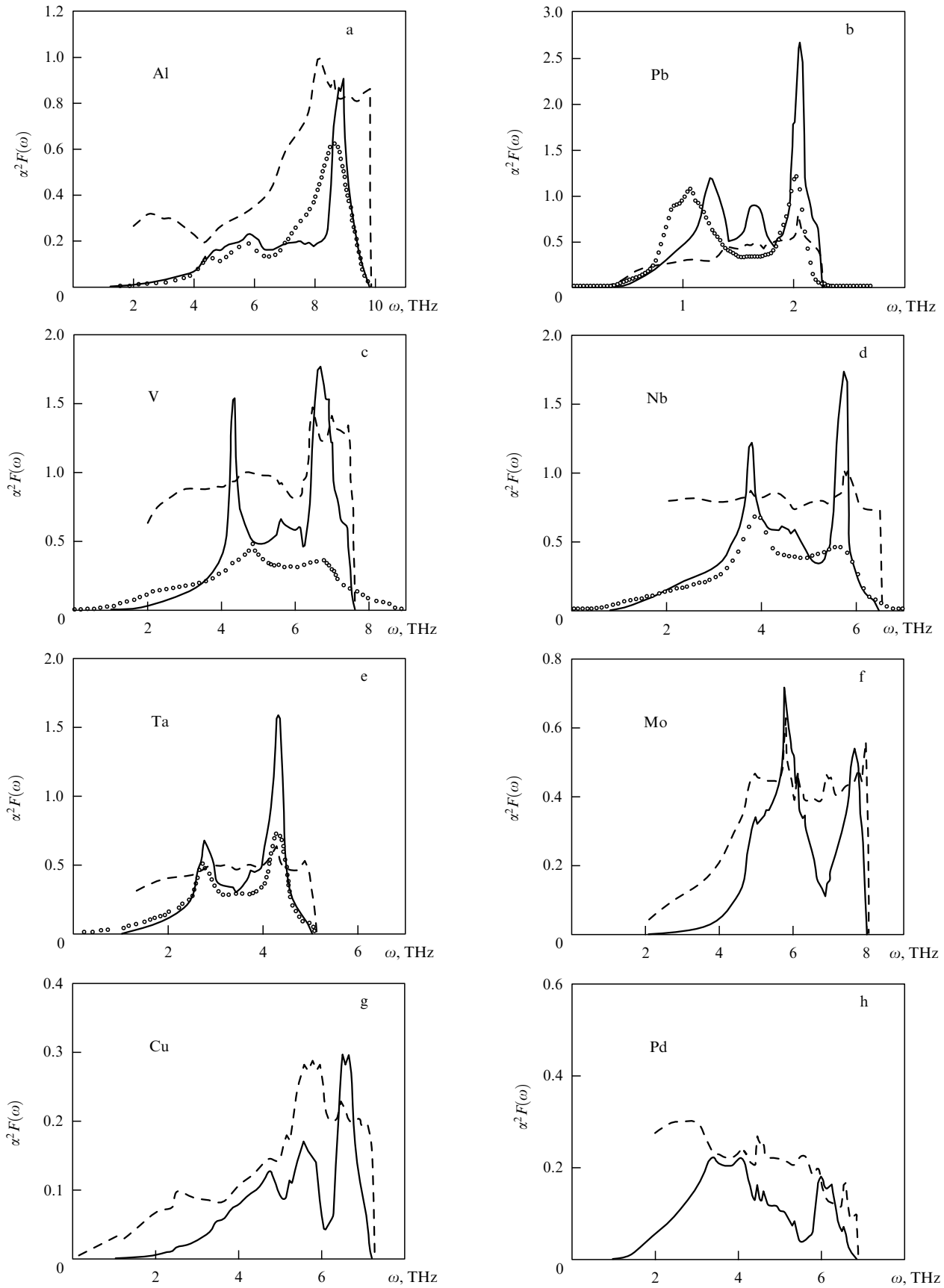

Figure 1. Calculated spectral electron – phonon coupling functions $\alpha^2F(\omega)$ (solid line) and $\alpha^2(\omega)$ (dashed line) in Al (a), Pb (b), V (c), Nb (d), Ta (e), Mo (f), Cu (g), and Pd (h). Tunnelling data for Pb and Nb [50] are shown by circles.

Nb, this metal is less prone to oxidation, and therefore is more suitable for tunnelling experiments. In Ref. [53], $\lambda_{\rm tun}$ was found to be 0.78 which agrees with the theoretical results within the accuracy of our calculations, i.e. 10%. The agreement between the theoretical value and $\lambda_{\rm SH} = 0.83$ is still better. With this evidence in hand we cannot consider the drawbacks of the linear response technique or the DFT local approximation to be responsible for the discrepancy with the tunnelling data for V and Nb. This is supported by the alternative estimates of EPI constants $\lambda_{\rm SH} = 1.17$ for both V and Nb, which were obtained from the data on heat capacity measurements. This value is well within the indicated limits of 10%. Moreover, the renormalization of a cyclotron mass in experiments on de Haas – van Alfvén effect [61] corresponds to $\lambda_{\rm dHvA} = 1.33$ for Nb, which is also close to our value of 1.26. Besides, our calculations reproduce anisotropy of the renormalization parameter on various sheets of the Fermi surface in Nb metal: (1) octahedron, $\lambda^{(1)} = 1.44$; (2) 'jungle', $\lambda^{(2)} = 1.37$; (3) ellipsoid $\lambda^{(3)} = 1.08$. These values can be compared to those given in Ref. [61]: $\lambda^{(1)}_{\rm dHvA} = 1.71$; $\lambda^{(2)}_{\rm dHvA} = 1.43$; $\lambda^{(3)}_{\rm dHvA} = 1.10$. (Notice that the anisotropy of the renormalization parameter obtained in RMTA calculations differs considerably from the results of Ref. [61] indicated above.) Subsequently some other evidence to support the suitability of the EPI approach in hand for Nb and V metals will be shown. But even now the difference between the theoretical and tunnelling results does not seem crucial if we take into account the current state of tunnelling experiments in Nb and V metals and the tendency of the tunnelling estimates of the coupling constant to increase as the procedure of the tunnelling data processing further improves.

Another two objects to which the suggested EPI description can apply are Mo and Cu metals. Tunnelling data on these metals is not available on account of weak electron – phonon effects and rather low critical temperatures. Our results for Mo calculated by both the linear response theory and the RMTA approximation coincide with the data of Ref. [62], and the coupling constant is estimated as $\lambda = 0.42$, which correlates with $\lambda_{\rm SH} = 0.45$, obtained from the heat capacity measurements. The calculated value for Cu is $\lambda = 0.14$. So far experimental estimates of this quantity in Cu are lacking.

Palladium provides the last illustration. This metal is noted for its strong spin fluctuations, so it is not a superconductor. Tunnelling data on Pd are also lacking. The paramagnon contribution into the mass renormalization shows up in the electron heat capacity $\lambda_{\rm SH} = \lambda + \lambda_{\rm spin} = 0.69$, which makes impossible the direct comparison of data related to EPI effects. Comparing this value with the calculated EPI constant $\lambda = 0.35$, we estimate the paramagnon contribution as $\lambda_{\rm spin} = 0.34$, which agrees well with the previous estimates at a level of 0.31 obtained by RMTA calculations [63]. We will return to this problem when discussing the superconducting state and now let us consider how the approach suggested applies to the description of kinetic phenomena in the normal phase.

The electron – phonon scattering contributes significantly to the electrical and thermal resistivities of metals outside the rather low temperatures at which the processes of impurity and electron – electron scattering come into importance. The EPI influence on the transport properties of metals is described by the transport spectral function which was introduced earlier by (39), (40). In the lower order approximation of the variational solution to the Boltzmann equation the expressions for electric and thermal resistivities have the form [64]

$$\rho = \frac{\pi\Omega_{\rm cell} k_{\rm B} T}{N(\varepsilon_{\rm F})\langle v_x^2\rangle} \int_0^\infty \frac{{\rm d}\omega}{\omega} \frac{x^2}{\sinh^2 x}\, \alpha^2_{\rm tr} F(\omega)\,, \tag{108}$$

$$w = \frac{6\Omega_{\rm cell}}{\pi k_{\rm B} N(\varepsilon_{\rm F})\langle v_x^2\rangle} \int_0^\infty \frac{{\rm d}\omega}{\omega} \frac{x^2}{\sinh^2 x} \times \left[\alpha^2_{\rm tr} F(\omega) + \frac{4x^2}{\pi^2}\, \alpha^2_{\rm out} F(\omega) + \frac{2x^2}{\pi^2}\, \alpha^2_{\rm in} F(\omega)\right], \tag{109}$$

where $x = \omega/2k_{\rm B}T$. The expression for electric resistivity completely coincides with that given by the generalized Drude formula (35) at $\omega = 0$. Determining the upper limit estimate of the electric resistivity as a variational solution, expression (108) nevertheless is sufficiently accurate to treat the electron – phonon interaction and calculate $\alpha^2_{\rm tr}F(\omega)$ by comparing theoretical and experimental data at intermediate temperatures. We calculated electric and thermal resistivities using formulas (108), (109) and our theoretical EPI spectra (40). It follows from (108), (109) that at high temperatures

$$\rho = \frac{\pi\Omega_{\rm cell} k_{\rm B} T}{N(\varepsilon_{\rm F})\langle v_x^2\rangle}\, \lambda_{\rm tr}\,, \tag{110}$$

$$w = \frac{6\Omega_{\rm cell}}{\pi k_{\rm B} N(\varepsilon_{\rm F})\langle v_x^2\rangle}\, \lambda_{\rm tr}\,, \tag{111}$$

where $\lambda_{\rm tr}$ is defined as

$$\lambda_{\rm tr} = 2\int_0^\infty \frac{{\rm d}\omega}{\omega}\, \alpha^2_{\rm tr} F(\omega)\,. \tag{112}$$

Expressions for $\alpha^2_{\rm tr}F(\omega)$ and $\alpha^2F(\omega)$ are very similar and differ only in the factor $1 - \mathbf{v}(\mathbf{k})\cdot\mathbf{v}(\mathbf{k}')/|\mathbf{v}(\mathbf{k})|^2$, which is characteristic of backscattering processes. Nevertheless, these functions can differ significantly in the case when the Fermi-surface areas are near parallel ('nesting') [65]. Despite the complicated shape of the Fermi surfaces in transition metals, our functions $\alpha^2_{\rm tr}F(\omega)$ are very similar to those shown in Fig. 1 (they are not presented in this review). Values of $\lambda_{\rm tr}$ are listed in Table 3. Comparison of these values with the data on EPI constants (Table 2) yields the difference between $\lambda_{\rm tr}$ and λ at a level of about 20% for all the studied materials. This completely agrees with the earlier made conclusion $\lambda_{\rm tr} \simeq \lambda$ [64] concerning transition metals. The temperature dependences of the electric resistivity $\rho(T)$ and thermal conductivity $w^{-1}(T)$ as compared to experimental ones are shown in Fig. 2 and Fig. 3, respectively. Of special interest is the intermediate temperature range $\Theta/5 < T < 2\Theta$, where $\Theta \sim \sqrt{\langle\omega^2\rangle_{\rm tr}}$. The expected lower-order corrections to the variational solution of the Boltzmann equation are small here, whereas the

Table 3. Theoretical transport constants $\lambda_{\rm tr}$ compared to experimental values determined from the data on electric resistivity and band calculations of plasma frequency $\omega_{\rm p}$, and average frequency $\Theta = \sqrt{\langle\omega^2\rangle_{\rm tr}}$.

Parameter	Al	Pb	V	Nb	Ta	Mo	Cu	Pd
$\lambda^{\rm calc}_{\rm tr}$	0.37	1.19	1.15	1.16	0.83	0.35	0.13	0.43
$\lambda^{\rm exp}_{\rm tr}$	0.39	1.52	1.15	1.11	0.93	0.40	0.12	0.50
$\omega_{\rm p}$, eV	12.29	14.93	7.95	9.47	9.05	8.81	8.75	7.34
Θ, K	330	75	260	200	170	290	230	190

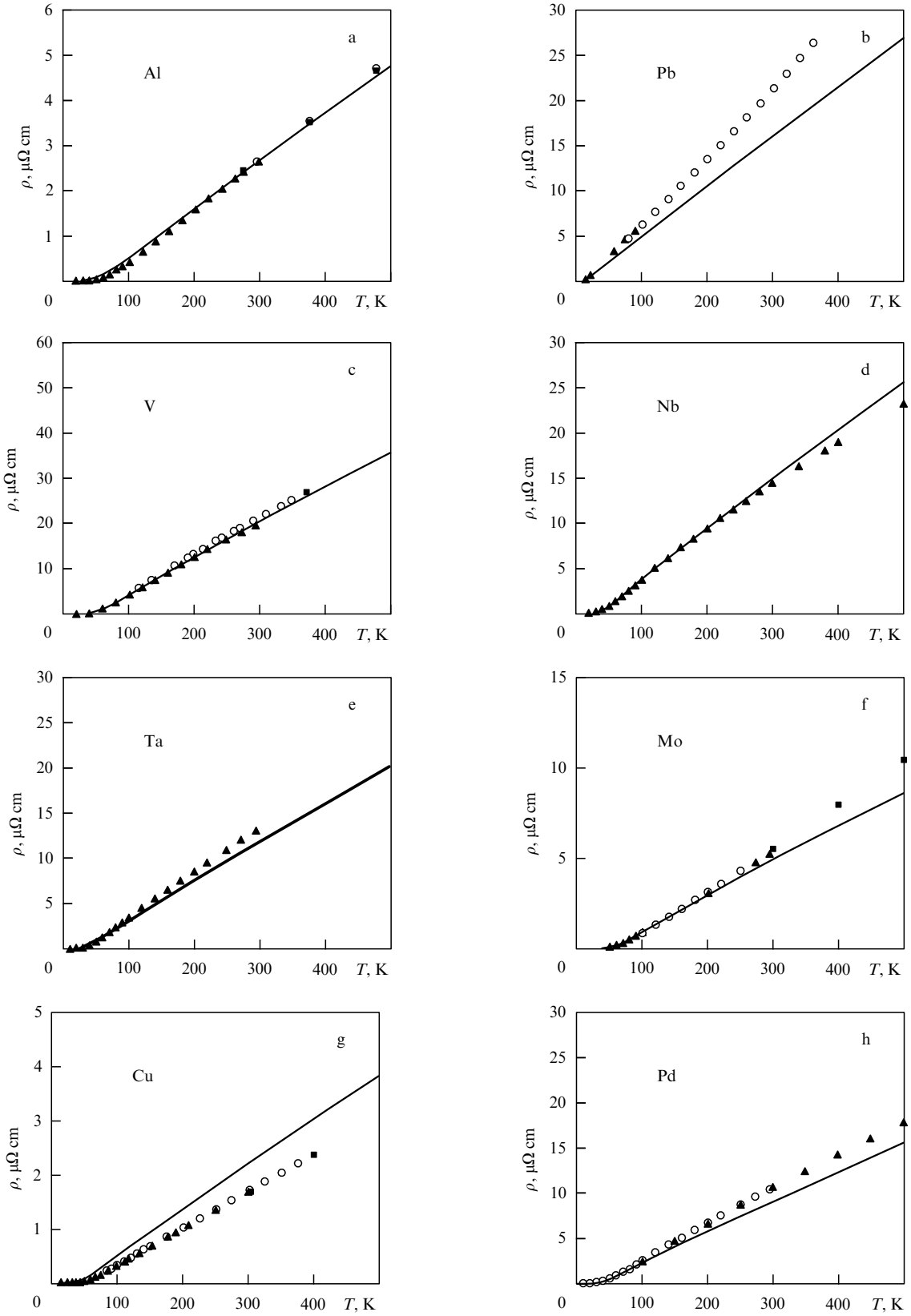

Figure 2. Temperature dependences of the phonon component of electric resistivity, calculated in the lower-order approximation to the variational solution of the Boltzmann equation in Al (a), Pb (b), V (c), Nb (d), Ta (e), Mo (f), Cu (g), and Pd (h) (solid lines). The experimental values (see Ref. [44], Table 15a) are shown by squares, circles, and triangles.

corrections for anisotropy and inelastic scattering can contribute considerably at low temperatures [64]. We have not analyzed the low-temperature $\rho(T)$ since a reliable value of $\alpha^2_{\rm tr}F(\omega)$ at $\omega \to 0$ is obtained by highly precise integration over the Brillouin zone, which is unattainable with our computer resources. The description of transport properties

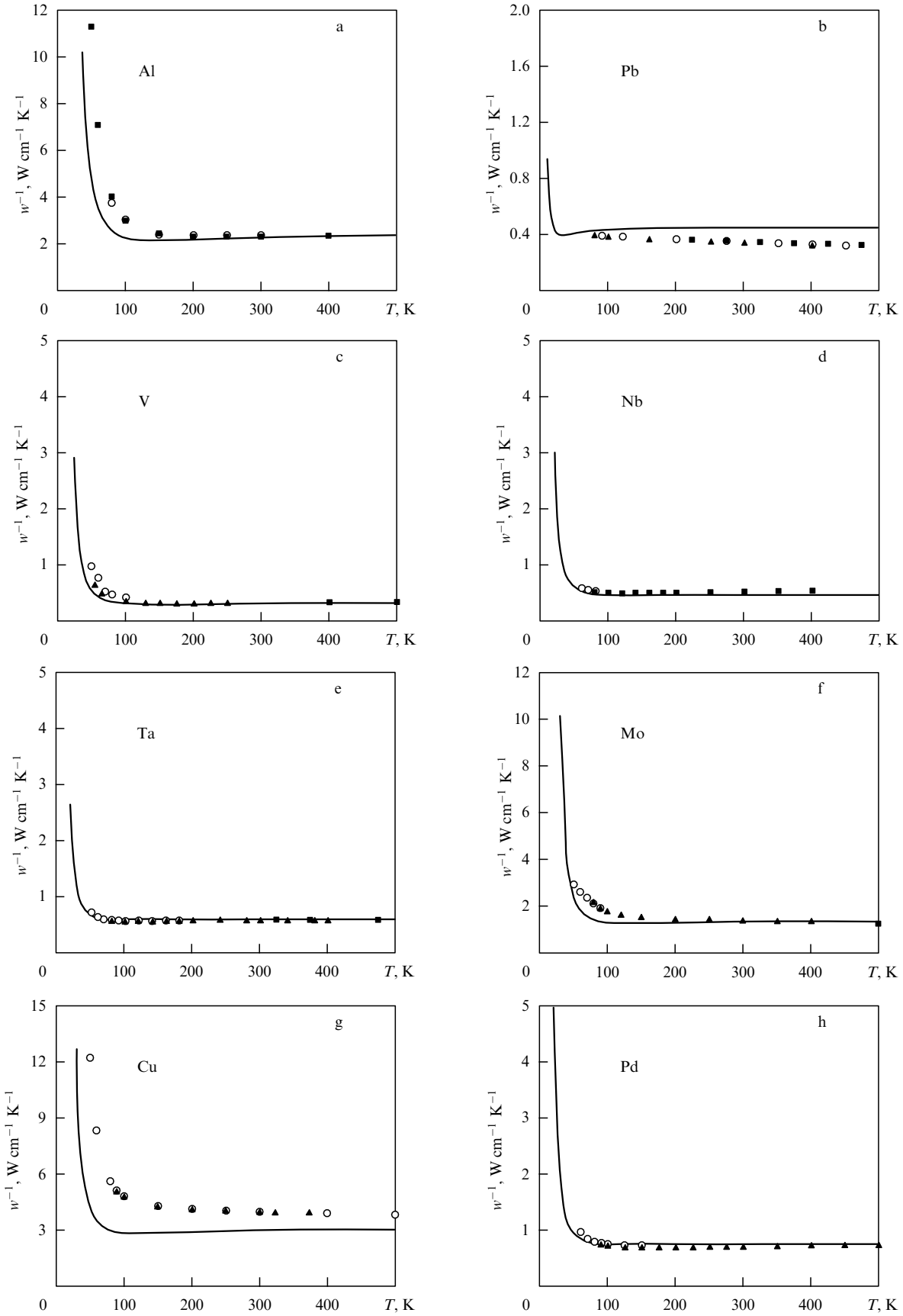

Figure 3. Temperature dependences of the phonon component of thermal conductivity, calculated in the lower-order approximation to the variational solution of the Boltzmann equation in Al (a), Pb (b), V (c), Nb (d), Ta (e), Mo (f), Cu (g), and Pd (h) (solid lines). The experimental values (see Ref. [44], Table 15c) are shown by squares, circles, and triangles.

at high temperatures ($T > 2\Theta$), in turn, requires the anharmonism and diffusive structure of the Fermi surface to be taken into account. Thus, the intermediate temperature range is best suited to study the relation between the transport properties and electron – phonon interaction. We determined the experimental values of $\lambda_{\rm tr}^{\rm exp}$ by polynomial interpolation of the experimental data shown in Fig. 2:

$$\rho(T) = \sum_{i=1}^{n} c_i T^{3-2i} \tag{113}$$

within the intermediate temperature range $\Theta/2 < T < \Theta$, $n = 2$. Increasing parameter n changes the coefficient c_1 of the linear term to within 3%. Experimental values of $\lambda_{\rm tr}^{\rm exp}$ were determined from the resultant coefficients c_1 and the data of our band calculations of plasma frequency $\omega_{\rm p}^2 = 16\pi N(\varepsilon_{\rm F})\langle v_x^2\rangle/\Omega_{\rm cell}$:

$$\lambda_{\rm tr}^{\rm exp} = \frac{c_1\omega_{\rm p}^2}{16\pi^2\Omega_{\rm cell}k_{\rm B}}\,. \tag{114}$$

The plasma frequencies, the calculated value of $\lambda_{\rm tr}^{\rm exp}$, and theoretical transport coupling constants $\lambda_{\rm tr}$ are listed in Table 3.

The experimental resistivity of Al (Fig. 2a) agrees with the theoretical one over the whole range of intermediate temperatures. The corresponding values of transport constants are $\lambda_{\rm tr}^{\rm exp} = 0.39$ and $\lambda_{\rm tr} = 0.37$. The difference of these constants from the EPI constant ($\lambda = 0.44$) just exceeds 10%. The curves of thermal conductivity (Fig. 3a) are also in good agreement at temperatures over $\Theta/5 \simeq 60$ K. As distinct from Al, the transport coupling constant of Pb equal to $\lambda_{\rm tr} = 1.19$ is noticeably less than the electron – phonon coupling constant $\lambda = 1.68$. This small value is probably caused by anisotropy effects which were neglected in the description of the kinetic properties of Pb, probably resulting in a more than 20% relative error in the calculated transport coupling constant with respect to the experimental one, $\lambda_{\rm tr}^{\rm exp} = 1.52$. As noted, the anharmonism effects can be significant in Pb. For lack of calculations based on a more exact solution to the Boltzmann equation we cannot identify the main cause of the discrepancy.

Of special interest is the description of kinetic properties of Nb, V and Ta metals, since comparison with the tunnelling data does not give an idea of the accuracy of our approach to the EPI calculation. The resistance measured in Nb exhibits saturation at high temperatures. Actually, this effect is noticeable (Fig. 2d) at temperatures over $2\Theta \simeq 400$ K and is not seen in the intermediate temperature range, where the resistance is slightly different from that predicted by the Boltzmann theory. Comparison between the calculated value $\lambda_{\rm tr} = 1.16$ and the empirical value $\lambda_{\rm tr}^{\rm exp} = 1.11$ yields the agreement to be about 5%. Vanadium also shows good agreement between experimental and theoretical data in the intermediate temperature range (the calculated value is $\Theta \simeq 260$ K). The theoretical estimate $\lambda_{\rm tr} = 1.15$ practically coincides with the derived value of $\lambda_{\rm tr}^{\rm exp}$, despite the fact that resistivity measured in V also reveals the saturation effect at high temperatures (not indicated in Fig. 2c). The suitability of formulas (108), (109) with a realistic spectral function for describing transport properties both in Nb and V metals is also supported by the data on thermal conductivity (Fig. 3d, c). These data yield similar estimates for $\lambda_{\rm tr}^{\rm exp}$ and numerical agreement between theoretical and experimental values, since the measured Lorentz number approaches the Sommerfeld one in the intermediate temperature range for $T \geqslant \Theta$. The agreement between the resistivity and thermal conductivity calculated for Ta (Fig. 2e and Fig. 3e) and those from measurements is not so good as for Nb and V. While the experimental and theoretical data on thermal conductivity correlated closely, our electric resistivity was underestimated by approximately 10 – 12%. As a consequence, the obtained value $\lambda_{\rm tr}^{\rm exp} = 0.93$ exceeded the theoretical estimate (0.83) for the Ta transport constant. This discrepancy can be attributed to high-temperature effects near the upper limit of the temperature range considered ($2\Theta \simeq 320$ K). Besides, the estimate of $\lambda_{\rm tr}^{\rm exp}$ obtained from available experimental data is not quite reliable, since the accuracy of detecting the electron – phonon component of the resistance depends on the sample purity and must be confirmed by several experiments.

For these reasons we did not consider the resistivity at temperatures over 300 K, shown in Fig. 2f for Mo metal. Interpolation over the range $T < 300$ K (the value calculated for Mo was $\Theta \simeq 280$ K) yields the empirical transport constant to be $\lambda_{\rm tr}^{\rm exp} = 0.40$, which coincides with our prediction. The agreement between data on thermal conductivity was satisfactory over the whole temperature range shown in Fig. 3f. For lack of tunnelling data on Cu we were not able to compare the electron – phonon coupling constants for this metal immediately. The agreement between the transport constants $\lambda_{\rm tr} = 0.13$ and $\lambda_{\rm tr}^{\rm exp} = 0.12$ was quite satisfactory.

The achieved accuracy 10 – 13% of calculated transport properties in Pd metal (Fig. 2h and Fig. 3h) and the corresponding coupling constants (see Table 3) is just higher than the accuracy of our numerical estimates. As distinct from Ta, this discrepancy can be most likely explained by additional resistance mechanisms occurring in Pd.

It follows from the above data that the observed behaviour of $\rho(T)$ and $w(T)$ corresponds to relationships (110) and (111) over the intermediate temperature range, and the theoretical curves calculated with realistic transport EPI functions are largely in good agreement with the experimental data. More precisely, the values of $\lambda_{\rm tr}^{\rm exp}$ obtained from the experimental data with the use of band calculations of the plasma frequency $\omega_{\rm p}$ correlate with the theoretical estimates of transport constants to within 10%. For Nb, V, Mo, and Al metals the discrepancy is even less than 5%. Actually, the ratio $\lambda_{\rm tr}/\omega_{\rm p}^2$ was compared to the experiment. In the metals considered, except for Cu, the band calculations yield a good estimate of plasma frequency. Thus, we believe that the theoretical values of $\lambda_{\rm tr}$ do agree with the experimental ones, though the calculation accuracy could be further improved. Drawbacks of the lower-order variational solution of the Boltzmann equation, which does not include the anisotropy of electron – phonon scattering, along with the anharmonism effects could be responsible for the discrepancy observed in Pb metal. In treating the data on Pd, a possible additional mechanism of resistance was not taken into account either. Nevertheless, in view of the agreement between other parameters we believe the description of the electron – phonon interaction to be quite satisfactory for all the studied metals.

Now let us discuss the results of calculating the electron relaxation times caused by EPI. One of the most-used and available methods for the study of relaxation time is the optical measurement in the infrared region. Until recently, optical measurements were usually described by the so-called

Drude formula for conductivity [66]:

$$\sigma(\omega) = \frac{\omega_{\rm p}^2}{4\pi} \frac{1}{-{\rm i}\omega + \tau_{\rm tr}^{-1}} , \tag{115}$$

where $\tau_{\rm tr}^{-1}$ is the inverse relaxation time. This quantity was usually considered a constant. Since the measurements were generally taken at energies of optical quanta ω greatly exceeding the phonon frequencies and at rather high temperatures, the independence of $\tau_{\rm tr}^{-1}$ from ω was beyond question. This fact was substantially confirmed by theoretical calculations of the relaxation time being involved in the one-particle Green's function [see formula (26)]. It is well known [3] that the corresponding function τ^{-1} sharply increases with ω and tends to constant at $\omega \simeq \omega_{\rm max}$, where $\omega_{\rm max}$ is the maximal frequency of phonons.

In this regard the measurements of optical relaxation times gave surprising results in high-temperature superconductors (HTSC) [67]. The inverse relaxation time was shown to rise linearly with the energy ω over a wide energy range from 0.02 eV to 0.4 eV, though $\omega_{\rm max}$ is of the order of 0.1 eV in these compounds. Many researchers interpreted this behaviour of the function $\tau^{-1}(\omega)$ as evidence for the existence of an electron relaxation mechanism in HTSC, other than EPI. In particular, a model of a marginal Fermi liquid was suggested [68], whose behaviour at low energies differs drastically from that of a standard Landau's Fermi liquid. In truth, as was demonstrated in Ref. [69], such a behaviour of the relaxation time can easily be explained within the conventional EPI approach. The main reason of this phenomenon is that the one-particle relaxation time given by (21) and (25) differs significantly from the kinetic relaxation time involved in the generalized Drude formula (35) and determined with (36) and (37).

As is easy to see, both the inverse relaxation times behave similarly at high temperatures $T > \omega_{\rm max}$ and energies $\omega \gg \omega_{\rm max}$:

$$\frac{1}{\tau_{\rm tr}} = 2\pi\lambda_{\rm tr} T , \qquad T > \omega_{\rm max} , \tag{116}$$

$$\frac{1}{\tau_{\rm tr}(\omega)} = \pi\lambda_{\rm tr}\langle\omega\rangle_{\rm tr} , \qquad \omega \gg \omega_{\rm max} . \tag{117}$$

Here $\langle\omega\rangle$ and $\langle\omega\rangle_{\rm tr}$ are the corresponding average phonon frequencies determined as

$$\langle\omega\rangle_{\rm tr} = \frac{2}{\lambda_{\rm tr}} \int {\rm d}\omega\, \alpha_{\rm tr}^2(\omega) F(\omega) . \tag{118}$$

As already noted, in metals $\lambda \simeq \lambda_{\rm tr}$, though in some cases they can differ considerably. The behaviour of functions $\tau^{-1}(\omega)$ and $\tau_{\rm tr}^{-1}(\omega)$ can differ widely in the limit $T \to 0$ and $\omega \to 0$, but they both vanish in this limit. The most essential difference between these functions is observed in the intermediate range of energies and temperatures. Using the above calculated functions $\alpha^2(\omega)F(\omega)$ and $\alpha_{\rm tr}^2(\omega)F(\omega)$, we computed functions $\tau^{-1}(\omega)$ and $\tau_{\rm tr}^{-1}(\omega)$ for Pb, Nb, and Al metals [70]. Figure 4a shows the frequency-dependent inverse relaxation times for Pb at temperatures $T = \Theta/10, \Theta/2, \Theta$. We do not present dependences for Nb, since they are virtually indistinguishable from those for Pb in the scale used. Figure 4a also shows the data for $\tilde{\tau}^{-1}(\omega)$ given by

$$\frac{1}{\tilde{\tau}(\omega)} = \frac{m}{m^*(\omega)} \frac{1}{\tau(\omega)} . \tag{119}$$

According to the analysis of Section 2, these data more adequately represent the idea of an inverse relaxation time, as well as being more usually obtained in experiments [67].

As seen from the figure, the behaviour of functions $\tilde{\tau}^{-1}(\omega)$ and $\tilde{\tau}_{\rm tr}^{-1}(\omega)$ does differ drastically in the range of intermediate energies. Thus, for example, $\tilde{\tau}_{\rm tr}^{-1}$ does not reach its maximal value $\pi\lambda_{\rm tr}\langle\omega\rangle_{\rm tr}$ even at energies $\omega \simeq 10\Theta$. Moreover, in the energy range $\Theta/5 \leqslant \omega \leqslant 3\Theta$ the function $\tilde{\tau}_{\rm tr}^{-1}(\omega)$ increases quasi-linearly with ω. The same behaviour of these functions is exhibited by Al (Fig. 4b), though the EPI constant of this metal is much less than that of Pb. The only point to be mentioned is that the region of quasi-linear behaviour of the function $\tilde{\tau}_{\rm tr}^{-1}(\omega)$ is slightly more narrow in this case. As shown in Ref. [69], in HTSCs, where the EPI constant λ can be of the order of 2, the region of the quasi-linear dependence for $\tilde{\tau}_{\rm tr}^{-1}(\omega)$ can extend up to $\omega \simeq 4\Theta$. Thus, the quasi-linear dependence of $\tilde{\tau}_{\rm tr}^{-1}(\omega)$ is a common property of all metals, caused by EPI. The difference between metals is only due to the various energy ranges determined by the EPI constant and the maximal phonon energy.

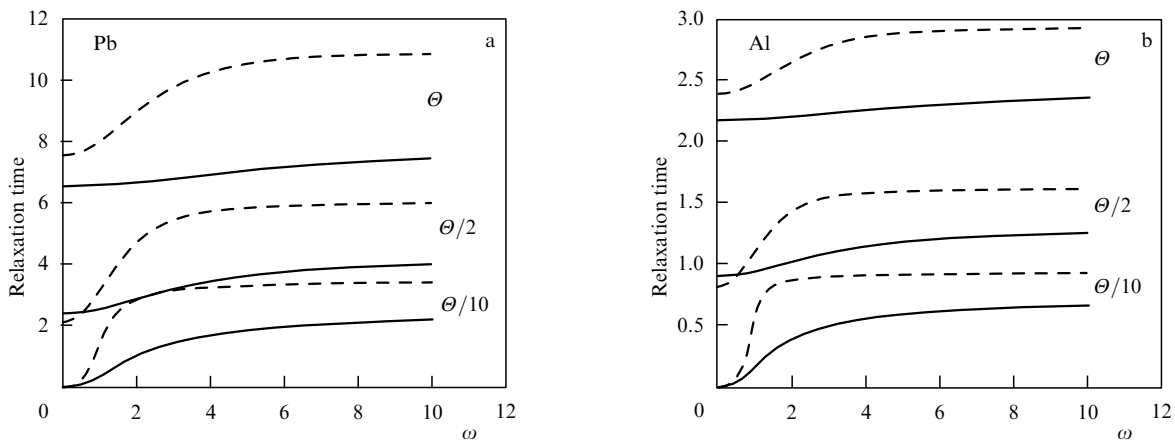

Figure 4. Effective lifetimes $\tilde{\tau}^{-1}(\omega)$ (dashed lines) and kinetic inverse relaxation times $\tilde{\tau}_{\rm tr}^{-1}(\omega)$ (solid lines) in Pb (a) and Al (b). The calculated data were gleaned from the theoretical EPI spectral functions depending on the frequency ω at three different temperatures T: $\Theta/10$, $\Theta/2$, Θ. The dimensionless frequency is quoted in $\omega_{\rm max}$ units.

To conclude this section, let us discuss the results of the numerical solution to Eliashberg equations with theoretical spectral functions $\alpha^2F(\omega)$. Notice that in the case of the linearized Eliashberg equation, the transition temperature T_c has long been known to be expressed by McMillan's interpolation formula derived in calculations with the model spectral function:

$$T_c = \frac{\langle\omega_{\log}\rangle}{1.2}\exp\left[-\frac{1.04(1+\lambda)}{\lambda-\mu^*(1+0.62\lambda)}\right]. \qquad (120)$$

It is seen that the first inverse moment of the spectral function λ and the quantity μ^* have a profound effect on T_c. As already noted, the Coulomb pseudopotential μ^* is poorly known, and actually can be used as a fitting parameter. We determined the quantity μ^*, taking the critical temperature equal to the experimental one and numerically solved the Eliashberg equation for T_c, or more precisely, for μ^*. The parameter ω_c was chosen to be $10\omega_{\max}$. Thus, the Coulomb repulsion parameter was referred to the same frequency value, i.e. $\mu^*(\omega_c)$. To consider the Coulomb pseudopotential parameter in the context of expression (120), the parameter $\mu^*(\omega_c)$ actually used in solving the Eliashberg equation, must be reduced to $\mu^* = \mu^*\big(\langle\omega_{\log}\rangle\big)$ by the formula

$$\frac{1}{\mu^*} = \frac{1}{\mu^*(\omega_c)} + \ln\frac{\omega_c}{\langle\omega_{\log}\rangle}. \qquad (121)$$

Our calculated results are presented in Table 4, which also lists the values of T_c^M computed using formula (120). The energy gap Δ_0 at $T=0$, obtained numerically from the Eliashberg equation for the gap, was taken as a parameter to be compared with experiment. The parameter μ^* was already specified by the correct value of T_c.

Table 4. Calculated values of μ^* fitting experimental data on T_c under the numerical solution to the Eliashberg equation with theoretical spectral functions $\alpha^2F(\omega)$. Data on T_c^M are determined by McMillan's formula to detect the difference between the exact numerical solution and interpolation. Calculated and experimental [50] energy gaps Δ_0.

Parameter	Al	Pb	V	Nb	Ta	Mo	Cu	Pd
μ^*	0.12	0.17	0.30	0.21	0.17	0.16	0.11	—
$T_c^{\exp}$, K	1.18	7.19	5.40	9.25	4.47	0.92	>0	—
T_c^M, K	1.40	6.90	6.68	10.12	4.91	1.07	>0	—
Δ_0^{calc}, meV	0.18	1.35	0.84	1.53	0.70	0.14	—	—
$\Delta_0^{\exp}$, meV	0.18	1.33	0.81	1.56	0.71	—	—	—

The tunnelling data available for Al yield $\Delta_0 = 0.18$ meV, which coincides with our result. The corresponding value $2\Delta_0/T_c = 3.54$ practically matches that given by the Bardeen – Cooper – Schriffer theory. Besides, the value $\mu^* = 0.12$ corresponds to the usual estimates for simple metals. The difference between the exact solution $T_c = 1.18$ K and that predicted by McMillan's formula, i.e. $T_c^M = 1.22$ K, is less than 5%, which is not surprising, because a simple spectrum of Al (Fig. 1a) is well approximated by the model functions. Of still more interest is the result obtained for Pb, where the spectrum already exhibits distinct double peaks (Fig. 1b). Nevertheless, formula (120) is still accurate to within 5% and yields $T_c^M = 6.81$ K, whereas $T_c = 7.19$ K. Known as a system with strong electron – phonon coupling among the studied metals, Pb possesses the maximal ratio $2\Delta_0/T_c \simeq 4.3$. The numerical solution to the Eliashberg equation yields the energy gap $\Delta_0 = 1.35$ meV, which practically coincides with the tunnelling estimates $\Delta_0^{\exp} = 1.33$ meV. However, our value $\mu^* = 0.17$ could be regarded as too high. The same situation holds for transition metals.

We used $\mu^* = 0.17$ for Ta and got $\Delta_0 = 0.70$ meV, which is comparable with the experimental finding of 0.71 meV. In the transition metals of interest, which have a pronounced double-peak EPI spectrum (see Fig. 1) with rather a large amplitude, McMillan's formula yields an accuracy of less than 10%. This necessitates an exact solution to the Eliashberg equation for T_c. In Ta ($T_c = 4.47$ K), V ($T_c = 5.40$ K), and Nb ($T_c = 9.25$ K) metals the corresponding values of T_c^M are 5.11, 6.68, and 10.5 K, respectively. Despite the difficulties in making tunnelling experiments on Nb and V metals, and the ensuing variety of results (which was mentioned in discussing the data concerning the estimation of the coupling constant λ), the energy gap is almost the same in all the experiments. Thus, for V the experimental energy gap is $\Delta_0^{\exp} = 0.81$ meV. The calculated value is 0.84 meV, exceeding the experimental one by only 4%. In Nb, the experimental value 1.56 meV practically coincides with the theoretical 1.53 meV. The Coulomb pseudopotential parameter μ^* is the most difficult to study in these metals. According to our scheme, we took the Coulomb pseudopotential parameters in V and Nb to be 0.29 and 0.21, respectively. It must be said that the parameter μ^*, whose magnitude was evaluated from the tunnelling data, is overestimated due to the fact that theoretical data on the coupling constants λ exceed the corresponding tunnelling estimates. As a consequence, higher values of μ^* are required to yield the proper transition temperature. This problem has been discussed in literature (see, for example, Ref. [71]), in particular, in the context of the possibility of spin fluctuations in Nb and V metals. Since paramagnons suppress the critical temperature, the observed values of T_c for high theoretical EPI constants can probably be explained without assuming large values of μ^*. But in this case a contribution of λ_{spin} to the renormalization of the electron mass should also arise due to electron-paramagnon interaction. As seen from Table 2, the experimental values of λ_{SH} exactly coincide with λ calculated for phonons, leaving no room for the paramagnon contribution λ_{spin} (except for Pd). On the other hand, the values of $\mu^* < 0.3$ can still be considered appropriate.

In conclusion, let us discuss the results for Mo, Cu, and Pd metals. Tunnelling data on Mo are lacking due to its small critical temperature. The calculated value is $\Delta_0 = 0.14$ meV, which is not surprising bearing in mind that superconductivity in Mo is close to the Bardeen – Cooper – Schriffer model, and results in $2\Delta_0/T_c = 3.53$. The estimate 0.14 for μ^* is also commonly accepted. The Coulomb repulsion parameter calculated for Cu (which is sufficient to suppress the superconductivity) is $\mu^* = 0.11$. As for Pd, the earlier calculated value of $\lambda_{\text{spin}} = 0.34$ practically coincides with the electron – phonon coupling constant $\lambda = 0.35$, which corresponds to the commonly accepted idea of superconductivity suppression in this metal.

6. Conclusions

In this review we have shown that in standard metals with small adiabatic parameter $(\omega_D/\varepsilon_F)^{1/2}$, the EPI problem can be solved practically exactly in the framework of the many-body Migdal – Eliashberg theory for both normal and super-

conducting states. This fact is not new, having been known since the earliest papers by Migdal [13] and Eliashberg [14].

As was repeatedly emphasized in Rainer's recent papers [2, 72], in the framework of Landau's Fermi-liquid theory the electron – phonon interaction and its contribution to the physical properties of metals is completely described by several spectral densities, in particular, by the Eliashberg function $\alpha^2(\omega)F(\omega)$. Within the Fermi-liquid theory these densities remain undetermined material parameters (more precisely, functions) of a particular metal. We have shown that the EPI calculations using the DFT [39, 41 – 43], which have been developed recently, enable one to calculate the spectral densities with rather high accuracy. We have also demonstrated that the hybrid calculation methods based on the substitution of the EPI matrix element (calculated by the DFT) into the formulas of the many-body theory, apply only for standard metals. The question arises of how we can identify a particular metal as standard or nonstandard and what are nonstandard metals. Above all, the standard metals are, in a sense by definition, the ones in which the adiabatic parameter is met *a priori*. The adiabaticity can be violated as a result of rather trivial reasons. For example, in the case of degenerate semiconductors the Fermi energy of conduction electrons can appear comparable to the characteristic phonon frequencies. This can give rise to various hybrid electron – phonon excitations and other nonadiabatic phenomena. Another reason of nonadiabaticity, which is also rather trivial, can be intensive interband transitions with energies comparable to phonon frequencies. Clearly, *ab initio* calculations of the phenomena arising even in these simple cases are impossible at the moment. Moreover, the possibility of using the Fröhlich Hamiltonian with a specified EPI matrix element does not seem obvious even for the qualitative study of these nonadiabatic phenomena.

Even more uncertain is the situation with systems displaying strong exchange-correlation effects. The studies performed to date [73 – 76] have used a semiphenomenological approach, where interelectron interactions are described by the Hubbard model. In these circumstances it is difficult to establish a relation between the results of the band DFT and the data of model calculations. No less difficult is to reveal a real difference between the EPI calculations by the DFT and the experiment in such systems, since the methods described in this review have been used so far to calculate only one system, i.e. $CaCuO_2$ [77], suspected of possible strong exchange-correlation effects. However, little evidence has been accumulated on the kinetic and optical properties of this system.

In conclusion the authors express their gratitude to many colleagues for the discussion of this review. We are especially grateful to O V Dolgov, K A Kikoin, M Kulich, and D Rainer. This work was supported by the grants of INTAS (93-2154) and the Russian Foundation for Basic Research (96-02-16134a).

References

1. Scalapino D J, in *Superconductivity* Vol. 1 (Ed. R D Parks) (New York: Dekker, 1969) p. 449
2. Rainer D, in *Progress in Low-Temperature Physics* (Ed. D F Brewer) (Amsterdam: Elsevier, 1986) p. 371
3. Allen P B, Mitrovic B, in *Solid State Physics* Vol. 37 (Eds F Seitz, D Turnbull, H Ehrenreich) (New York: Academic Press, 1982) p. 1
4. Dolgov O V, Maksimov E G *Tr. Fiz. Inst. Akad. Nauk SSSR* **148** 3 (1983)
5. McMillan W L, Rowell J M, in *Superconductivity* Vol. 1 (Ed. R D Parks) (New York: Dekker, 1969) p. 561
6. Gaspari G D, Gyorffy B L *Phys. Rev. Let.* **28** 801 (1972)
7. Hohenberg P, Kohn W *Phys. Rev.* **136** B864 (1964)
8. Kohn W, Sham L J *Phys. Rev.* **140** A1133 (1965)
9. Lundqvist S, March S N (Eds) *Theory of the Inhomogeneous Electron Gas* (New York: Plenum, 1983) [Translated into Russian (Moscow: Mir, 1987)]
10. Savrasov S Yu, Maksimov E G *Usp. Fiz. Nauk* **165** 773 (1995) [*Phys. Usp.* **38** 737 (1995)]
11. Gross E K U, Dobson J F, Petersilka M, in *Density Functional Theory* (Topics in Current Chemistry, Ed. R F Nalewaiski) (Berlin: Springer-Verlag, 1996) p. 71
12. Abrikosov A A, Gor'kov L P, Dzyaloshinskiĭ I E *Metody Kvantovoĭ Teorii Polya v Statisticheskoĭ Fizike* (Methods of Quantum Field Theory in Statistical Physics) (Moscow: Fizmatgiz, 1962) [Translated into English (Englewood Cliffs, NJ: Prentice-Hall, 1963)]
13. Migdal A B *Zh. Eksp. Teor. Fiz.* **34** 1438 (1958) [*Sov. Phys. JETP* **34** 996 (1958)]
14. Eliashberg G M *Zh. Eksp. Teor. Fiz.* **38** 966 (1960); **39** 1437 (1960) [*Sov. Phys. JETP* **11** 696 (1960); **12** 1000 (1961)]
15. Allen P B, in *Dynamical Properties of Solids* Vol. 3 (Eds G K Horton, A A Maradudin) (Amsterdam: North-Holland, 1980) p. 95
16. Allen P B *Phys. Rev. B* **6** 2577 (1972)
17. Maksimov E G, Savrasov S Yu *Usp. Fiz. Nauk* **160** 155 (1990) [*Sov. Phys. Usp.* (1990)]
18. Mahan G D *Phys. Rep.* **145** 251 (1987)
19. Allen P B *Phys. Rev. B* **3** 305 (1971)
20. Allen P B *Commun. Cond. Math. Phys.* **15** 327 (1992)
21. Dolgov O V, Shulga S V *J. Supercond.* **8** 611 (1995)
22. Maksimov E G *Zh. Eksp. Teor. Fiz.* **69** 2236 (1975) [*Sov. Phys. JETP* (1975)]
23. Landau L D *Zh. Eksp. Teor. Fiz.* **34** 262 (1958); **35** 97 (1958) [*Sov. Phys. JETP* **34** 182 (1958); **35** 70 (1959)]
24. Silin V P *Zh. Eksp. Teor. Fiz.* **38** 977 (1960) [*Sov. Phys. JETP* **11** 703 (1960)]
25. Kantorovich V *Zh. Eksp. Teor. Fiz.* **45** 1638 (1963) [*Sov. Phys. JETP* **18** 1125 (1964)]
26. Luttinger J M, Ward J C *Phys. Rev.* **118** 1417 (1960)
27. Luttinger J M *Phys. Rev.* **119** 1153 (1960)
28. Yasuhara H, Ousaka Y *Int. J. Mod. Phys. B* **6** 3089 (1992)
29. Eliashberg G M *Physica A* **200** 95 (1993)
30. Eliashberg G M, von der Linden W *Pis'ma Zh. Eksp. Teor. Fiz.* **59** 413 (1994) [*JETP Lett.* **59** 441 (1994)]
31. Nozieres P *Theory of Interacting Fermi Systems* (New York, W A: Benjamin Inc., 1964)
32. Jones R O, Gunnarsson O *Rev. Mod. Phys.* **61** 689 (1989)
33. Sternheimer R M *Phys. Rev.* **96** 951 (1954); **107** 1565 (1957)
34. Zeĭn N E *Fiz. Tverd. Tela* (Leningrad) **26** 3028 (1984) [*Sov. Phys. Solid State* **26** 1825 (1984)]
35. Baroni S, Giannozzi P, Testa A *Phys. Rev. Lett.* **58** 1861 (1987)
36. Klein B M, Pickett W F, in *Superconductivity in d- and f-Band Metals* (Eds W Buckel, W Weber) (Karlsruhe: Kernforschungszentrum, 1982) p. 447
37. Butler W H, in *Physics of Transition Metals* (New York: AIP, 1980) p. 505
38. Schönhammer K, Gunnarsson O *Phys. Rev. B* **37** 3128 (1988)
39. Savrasov S Yu *Phys. Rev. Lett.* **69** 2819 (1992)
40. Andersen O K *Phys. Rev. B* **12** 3060 (1975)
41. Savrasov S Y, Savrasov D Y *Phys. Rev. B* **46** 12181 (1992)
42. Savrasov S Y, Savrasov D Y, Andersen O K *Phys. Rev. Lett.* **72** 372 (1994)
43. Savrasov S Y, Savrasov D Y *Phys. Rev. B* **54** 16487 (1996)
44. *Numerical Data and Functional Relationship in Science and Technology, Landolt-Börnstein New Series, Group III, Crystal and Solid State Physics* Vol. 13a (Ed. K-H Hellwege) (Berlin, New York: Springer-Verlag, 1981); Vol. 15a (Ed. K-H Hellwege) (1982), Vol. 15c (Ed. O Madelung) (1982)
45. Jepsen O, Andersen O K *Phys. Rev. B* **29** 5965 (1984)
46. Butler W H, Smith H G, Wakabayashi N *Phys. Rev. Lett.* **39** 1004 (1977); Butler W H, Pinski F J, Allen P B *Phys. Rev. B* **19** 3708 (1979)
47. Harmon B N, Sinha S K *Phys. Rev. B* **16** 3919 (1977); Glötzel B, Rainer D, Schober H R *Z. Phys. B* **35** 317 (1979); Peter M et al., in

Superconductivity in d- and f-Band Metals (Eds W Buckel, W Weber) (Karlsruhe: Kernforschungszentrum, 1982) p. 515
48. Winter H *J. Phys. F* **11** 2283 (1981)
49. Dacorogna M M, Cohen M L, Lam P K *Phys. Rev. Lett.* **55** 837 (1985)
50. Wolf E L *Principles of Electronic Tunnelling Spectroscopy* (Oxford: Oxford University Press, 1985)
51. de Gironcoli S *Phys. Rev. B* **51** 6773 (1995)
52. McMillan W L *Phys. Rev.* **167** 331 (1968)
53. Shen L Y *Phys. Rev. Lett.* **24** 1104 (1970)
54. Arnold G B, Zasadzinski J, Wolf E L *Phys. Lett. A* **69** 136 (1978); Wolf E L et al. *J. Low Temp. Phys.* **40** 19 (1980)
55. Zasadzinski J et al. *Phys. Rev. B* **25** 1622 (1982)
56. Geschneidner K A, in *Solid State Physics* Vol .16 (Eds H Ehrenreich, F Seitz, D Turnbull) (New York: Academic Press, 1964) p. 275
57. Radebaugh R, Keesom P H *Phys. Rev.* **149** 217 (1966)
58. Bostock J et al. *Phys. Rev. Lett.* **36** 603 (1976)
59. Gärtner K, Hahn A *Z. Naturforsch.* **31A** 861 (1976)
60. Robinson B, Geballe T H, Rowel J W, in *Superconductivity in d- and f-Band Metals* (New York: AIP Conf., 1972) p. 381
61. Crabtree G W et al. *Phys. Rev. Lett.* **42** 390 (1979)
62. Wolf E L *Principles of Electronic Tunnelling Spectroscopy* (Oxford: Oxford University Press, 1985) p. 263
63. Pinski F J, Butler W H *Phys. Rev. B* **19** 6010 (1979)
64. Pinski F J, Allen P B, Butler W H *Phys. Rev. B* **23** 5080 (1981)
65. Grespi V H, Cohen M L *Solid State Commun.* **81** 187 (1992)
66. Motulevich G P *Usp. Fiz. Nauk* **97** 211 (1969) [*Sov. Phys. Usp.*]
67. Rotter L D et al. *Phys. Rev. Lett.* **67** 2741 (1991); Cooper S L et al. *Phys. Rev. B* **4** 2549 (1992)
68. Schmitt-Rink S, Varma C M, Ruckenstein A E *Phys. Rev. Lett.* **60** 2793 (1988)
69. Shulga S V, Dolgov O V, Maksimov E G *Physica C* **178** 317 (1990)
70. Maksimov E G et al. (in press)
71. Rietschel H, Winter H *Phys. Rev. Lett.* **43** 1256 (1979)
72. Rainer D, in *Progress in Low-Temperature Physics* Vol. X (Ed. D E Brewer) (Amsterdam: Elsevier, 1986) p. 371
73. Kim J H et al. *Phys. Rev. B* **44** 5148 (1991)
74. Kim J H, Tesanovic Z *Phys. Rev. Lett.* **71** 4218 (1993)
75. Grilli M, Castellani C *Phys. Rev. B* **50** 16880 (1994)
76. Kulic M, Zeyher R *Phys. Rev. B* **49** 4395 (1994)
77. Savrasov S Yu, Andersen O K *Phys. Rev. Lett.* **77** 4430 (1996)